The evolution of ovary-specific gene expression in Hawaiian Drosophilidae

Samuel H. Church[1,2,*] Catriona Munro[3] Casey W. Dunn[2]
Cassandra G. Extavour[1,4,5]

[1] Department of Organismic and Evolutionary Biology, Harvard University, Cambridge, MA 02138, USA

[2] Current address: Department of Ecology and Evolutionary Biology, Yale University, New Haven, CT 06520, USA

[3] Collège de France, PSL Research University, CNRS, Inserm, Center for Interdisciplinary Research in Biology, 75005 Paris, France

[4] Department of Molecular and Cellular Biology, Harvard University, Cambridge, MA 02138, USA

[5] Howard Hughes Medical Institute, Chevy Chase, MD 20815

* corresponding author: samuelhchurch@gmail.com

1 Abstract

As detailed data on gene expression become accessible from more species, we have an opportunity to test the extent to which our understanding of developmental genetics from model organisms helps predict expression patterns across species. Central to this is the question: how much variation in gene expression do we expect to observe between species? Here we provide an answer by comparing RNAseq data between twelve species of Hawaiian Drosophilidae flies, focusing on gene expression differences between the ovary and other tissues. We show that there exists a cohort of ovary-specific genes that is stable across species, and that largely corresponds to described expression patterns from laboratory model *Drosophila* species. However, our results also show that, as phylogenetic distance increases, variation between species overwhelms variation between tissues. Using ancestral state reconstruction of expression, we describe the distribution of evolutionary changes in tissue-biased expression profiles, and use this to identify gains and losses of ovarian expression across these twelve species. We then use this distribution to calculate the correlation in expression evolution between genes, and demonstrate that genes with known interactions in *D. melanogaster* are significantly more correlated in their evolution than genes with no or unknown interactions. Finally, we use this correlation matrix to infer new networks of genes that have similar evolutionary trajectories, and we provide these as a dataset of novel testable hypotheses about genetic roles and interactions.

2 Introduction

Data on when and where genes are expressed are now fundamental to the study of development and disease[1]. With continually advancing RNA sequencing technologies, these data have been collected using RNA sequencing from a wide variety of cells, treatments and species[2,3]. Statistical analysis of gene expression across these differentials generates insights into how gene expression is connected to phenotypic differences in morphology and behavior[4]. However, when comparing gene expression across species, most studies have been restricted to pairwise comparisons, often between one model laboratory species and one other species of interest[5]. One challenge with such pairwise comparisons is that they lack robust information about how much evolutionary variation in expression we expect to observe, making it difficult to evaluate the significance of any interspecific difference in variation[5,6]. Instead, we need phylogenetic comparisons of expression that take into account the shared history between species[7,8], and that describe significant changes in expression in relation to other phenotypic traits of interest.[9] In this study we perform a phylogenetic comparison of gene expression across the organs of twelve species of Hawaiian Drosophilidae flies with highly divergent ovary and egg morphologies. From our results we identify individual genes that have undergone significant evolutionary shifts in organ-specific expression, and describe global patterns in transcriptome variation across species that can serve as a benchmark for future interspecific comparisons of gene expression.

Phylogenetic comparisons of developmental traits are particularly valuable for building context around comparisons between well-studied model organisms and their non-model relatives[10]. Much more has been learned about the genetics and development of laboratory model species like *D. melanogaster* than may ever be possible for the vast majority of life[11]. But the usefulness of model species to understand general principles depends in part on the extent to which biology in these species reflects the biology of other taxa, rather than species-specific phenomena[12]. In the case of gene expression, there has been substantial debate about the degree to which patterns observed in model organisms may be representative across species[13–16]. Where several studies showed that the expression profiles of organs within a species are more different the profiles of homologous organs across species[17–20], other work has questioned this finding[13,14]. More recently, Breschi and colleagues (2016)[21] demonstrated that, consistent with an evolutionary model of trait evolution, species-level variation in gene expression increases with the time since divergence from the most recent common ancestor. In addition, previous work by authors on this manuscript[8] showed that, while expression patterns across tissues tend to be consistent between species, lineage-specific shifts in expression enrichment can be identified by applying phylogenetic comparative methods. With the exception of the work by Munro and colleagues (2021)[8], these studies have been, to our knowledge, performed almost exclusively in vertebrate species[17,18,20], and for the most part placental mammals[13,14,16], meaning that far less is known about organ and species-level expression differences when comparing across the tree of life.

The detailed atlases of expression data across organs[22] and developmental timepoints[23] is one of the strengths of model systems like *D. melanogaster*. These public resources make it possible to explore global patterns of expression to gain insight into potential gene regulation, interaction, and function[23–25]. As atlases such as these have become increasingly detailed and available from more taxa, a new goal has been to compare these expression profiles across species[7,26,27]. One objective of these cross-species comparisons is to shed light on potential regulatory associations between genes[7,9]. This is especially advantageous for complex processes such as ovarian function for which we have a fragmented understanding of gene regulation despite genetic and transcriptome studies within single model organisms. Another objective of phylogenetic comparisons of expression atlases is to estimate the evolutionary distance between species at which we might expect a given gene to demonstrate a divergent pattern of expression[6]. If this distance is relatively small, then we predict atlases to contain large amounts of species-specific patterns. Alternatively, if as described above, variation across tissues outweighs variation across the species being compared, we predict atlases to contain large cohorts of tissue-specific genes that have been evolutionarily conserved. In this study we test for the existence of a core suite of ovary-specific genes across species of Hawaiian Drosophilidae and describe its size and composition in relation to the described atlas of expression in *D. melanogaster*.

The *Drosophila* ovary has several features[28] that make it a compelling organ in which to test hypotheses about expression evolution. Analyses of the FlyAtlas2 dataset[29] show that in *D. melanogaster*, more genes demonstrate highest expression enrichment in the ovary than any other adult organ (Fig. S1). Additionally,

all described signaling pathways are known to have a role in regulating ovarian development[30]. The ovary performs several critical functions, including maintaining the germ line and manufacturing specialized egg cells, yolk, and egg-shell materials[31]. Genetic screens[30,32] and experimental manipulation in *D. melanogaster* have revealed functions of many genes involved in these processes, including yolk-protein genes required for oogenesis[33] and embryonic patterning genes with localized mRNA like *nanos*[34] and *swallow*[35]. Here we compare whole-ovary RNA profiles to assess the extent to which these genes and others demonstrate consistent patterns of ovary-enrichment over evolutionary timescales in a clade with highly divergent ovary and egg morphologies.

The Hawaiian Drosophilidae clade contains an estimated 1,000 extant species[36] that diverged from a common ancestor with *D. melanogaster* between 25 and 40 million years ago[37]. Extant species have been studied in particular for the variation in ovary and egg morphology[38,39]. Species of Hawaiian Drosophilidae show the largest range within the family of egg size, shape, and the number of egg-producing units in the ovary, known as ovarioles[40–42]. Previous studies by our research group and others have shown that these traits are likely associated with evolutionary changes in the egg-laying substrate (e.g. rotting bark, flowers, leaves)[38,40]. Furthermore, our previous work demonstrated that at least one developmental process, governing how the number of ovarioles is specified in the adult *D. melanogaster* ovary, is conserved in Hawaiian *Drosophila*[40]. The diversity of Hawaiian species and their relationship to model species make them a strong candidate model clade for evo-devo research[36,43]. However, their relatively long generation times and species-specific breeding requirements make laboratory culture more challenging than classic *Drosophila* models[36]. In this study we leverage technologies that can be deployed on wild-caught individuals to gather rich developmental data to compare across species.

We compared the expression profiles of twelve species of wild-caught Hawaiian Drosophilidae species across three tissues: the adult ovary, head, and the remaining carcass (Fig. 1). First, we characterized the differentially expressed genes in the ovary of each species individually. By comparing these to each other, and to records of ovary-enriched genes from *D. melanogaster*, we identified a core suite of ovary genes shared across species. We then repeated this analysis for head-enriched genes, and compared the results across these parallel analyses to test the extent to which global patterns of expression difference are influenced by the identity of the tissues in question. We applied linear modeling to this dataset to test the overall contribution of species- and tissue-level differences to expression variation across genes, and describe the circumstances under which one is likely to dominate over the other. Finally, we used a phylogenetic analysis of expression changes over evolutionary time to identify genes likely to have gained and lost tissue-enriched expression. This evolutionary screen of expression changes allowed us to identify networks of genes that demonstrate correlated changes in expression evolution. We provide these networks as a searchable dataset of novel, testable hypotheses for gene regulation with respect to ovarian function. The results of this study demonstrate both the power of Hawaiian *Drosophila* as a model clade for evo-devo, and the potential of using phylogenetic methods to identify evolutionary variation in gene expression underlying phenotypic differences.

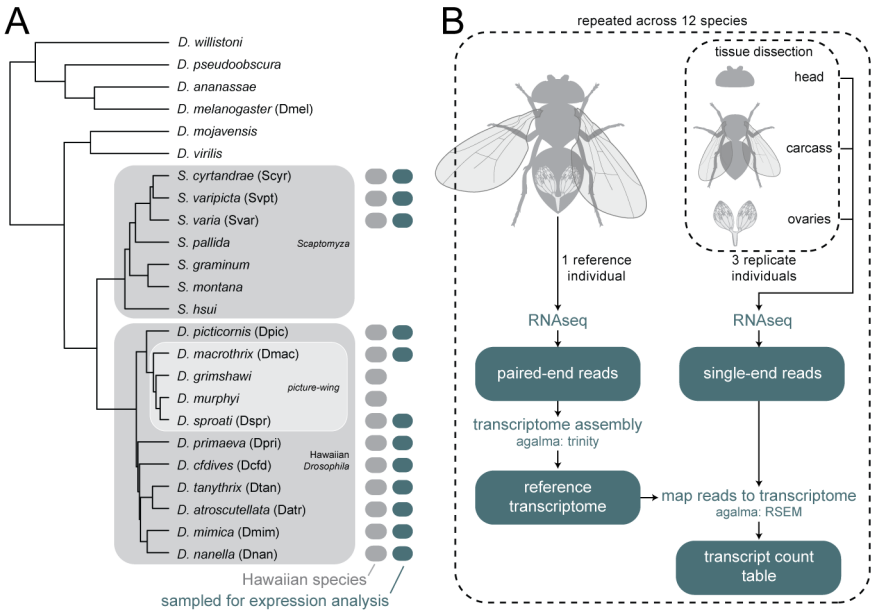

Figure 1: **Phylogeny of species and RNA sampling strategy.** A, Twelve species of Hawaiian Drosophilidae flies were collected in the wild and processed for RNA sequencing. The twelve reference transcriptomes assembled from these species were combined with twelve published genomes to generate the phylogeny shown here (originally published in Church and Extavour, 2021[44]). Three clades within the group are highlighted: the genus *Scaptomyza*, nested within the paraphyletic genus *Drosophila*; the Hawaiian *Drosophila*, which, along with *Scaptomyza*, make up the Hawaiian Drosophilidae; and the well-known *picture-wing* clade. Adjacent to tip labels are four letter species codes used throughout the manuscript. B, The experimental design used to generate the data in this manuscript. When sufficient specimens were available per species, one individual was used as a reference and three individuals were dissected into three separate tissues: the head, ovaries, and all remaining material (carcass). Reference individuals were sequenced to generate paired-end RNA reads and tissues were sequenced to generate single-end RNA reads. Tissue libraries were then mapped to the assembled reference to quantify transcript expression. Teal boxes indicate data files. Dashed-line boxes indicate a repeated step.

3 Methods

3.1 Field collection

Specimens used for transcriptome sampling were caught on the Hawaiian islands between May of 2016 and May of 2017. Specimens were caught using a combination of net sweeping and fermented banana-mushroom baits in various field sites on the Hawaiian islands of Kaua'i and Hawai'i (see Table S1 for locality data). Field collections were performed under permits issued by the following: Hawai'i Department of Land and Natural Resources, Hawai'i Island Forest Reserves, Kaua'i Island Forest Reserves, Koke'e State Park, and Hawai'i Volcanoes National Park. Adult flies were maintained in the field on vials with sugar media and kept at cool temperatures. They were transported alive back to Cambridge, MA where they were maintained on standard *Drosophila* media at 18°C. Samples were processed for RNA extraction between 5 and 31 days after collecting them live in the field (average 10.8 days, see Table S1). One species, *Scaptomyza varia*, was caught in the field before the adult stage by sampling rotting *Clermontia sp.* flowers (the oviposition substrate). For this species, male and female adult flies emerged in the lab, and were kept together until sampled for RNA extraction.

3.2 Species identification

Species were identified using dichotomous keys[45–49], when possible. Many keys for Hawaiian Drosophilidae are written focusing on male specific characters (e.g. sexually dimorphic features or male genitalia)[47]. Therefore, for species where females could not be unambiguously identified by morphology, we verified their identity using DNA barcoding. When males were caught from the same location, we identified males to species using dichotomous keys and matched their barcode sequences to females included in our study. We also matched barcodes from collected females to sequences previously uploaded to NCBI[50–52].

The following dichotomous keys were used to identify species: for *picture-wing* males and females, Magnacca and Price (2012)[45]; for *antopocerus* males, Hardy (1977)[46]; for *Scaptomyza*, Hackman (1959)[47]; for species in the *mimica* subgroup of MM, O'Grady and colleagues (2003)[48]; for other miscellaneous species, Hardy (1965)[49].

For DNA barcoding, DNA was extracted from one or two legs from male specimens using the Qiagen DNeasy blood and tissue extraction kit, or from the DNA of females isolated during RNA extraction (see below). We amplified and sequenced the cytochrome oxidase I (COI), II (COII) and 16S rRNA genes using the primers and protocols described in Sarikaya and colleagues (2019)[40].

For barcode matching, we aligned sequences using MAFFT, version v7.475[53], and assembled gene trees using RAxML, version 8.2.9[54]. Definitive matches were considered when sequences for females formed a monophyletic clade with reference males or reference sequences from NCBI; see Table S2.

Female *D. primaeva*, *D. macrothrix*, *D. sproati*, and *D. picticornis* could be identified unambiguously using dichotomous keys. Female *D. atroscutellata*, *D. nanella*, *D. mimica*, *D. tanythrix*, *S. cyrtandrae*, *S. varipicta*, and *S. varia* were identified by matching barcodes to reference sequences from NCBI, reference males, or both. For the female *haleakalae* fly used in this study, no male flies were caught in the same location as these individuals, and no other sequences for *haleakalae* males on NCBI were an exact match with this species. Given its similar appearance to *Drosophila dives*, we are referring to it here as *Drosophila* cf *dives*, and we await further molecular and taxonomic studies of this group that will resolve its identity.

3.3 Sampling strategy

The target number of mature, healthy female flies per species was four, with three intended for dissection and species specific expression libraries and one intended as a whole-body reference library (Fig. 1). When four such individuals were not available, a reference library was assembled by combining the tissue-specific libraries from one of the other individuals. This was the case for the following species: *D. sproati*, which was dissected and had RNA extracted separately from the head, ovaries, and carcass, with RNA combined prior to library preparation; and *S. varia*, *S. cyrtandrae* and *D.* cf *dives*, for which RNA was extracted and libraries prepared for separate tissues, and raw reads were combined after sequencing.

For the other eight species, sufficient individual females were available such that reads for transcriptome assembly were sequenced from a separate individual. In these cases one entire female fly was dissected and photographed to assess whether vitellogenic eggs were present in the ovary, and all tissues were combined in the same tube and used for RNA extraction. Library preparation failed for one individual *D. atroscutellata* fly, as well as two tissue-specific libraries: one head sample from *D. mimica*, and one head sample from *D. sproati*.

3.4 Dissection and RNA sequencing

Female flies were anesthetized in 100% ethanol and were dissected in a phosphate-buffered saline solution. The ovary was separated from the abdomen, and the head was separated from the carcass. Photographs of each tissue were taken, and tissues were moved to pre-frozen eppendorf tubes, kept in dry ice, and immediately transported to a -80°C freezer. Dissections were performed as quickly as possible to prevent

RNA degradation. Samples were stored at -80°C for between 90 and 336 days before RNA extraction (average 281.9 days, see Table S1).

RNA was extracted from frozen samples using the standard TRIzol protocol (http://tools.thermofisher.com/content/sfs/manuals/trizol_reagent.pdf). One mL of TRIzol was added to each frozen sample, which were then homogenized using a sterile motorized mortar. The recommended protocol was followed without modifications, using 10 µg of glycogen, and resuspending in 20µL RNAse-free water-EDTA-SDS solution. DNA for subsequent barcoding was also extracted using the phenol-chloroform phase saved from the RNA extraction.

RNA concentration was checked using a Qubit fluorometer, and integrity was assessed with a Agilent TapeStation 4200. RNA libraries were prepared following the PrepX polyA mRNA Isolation kit and the PrepX RNA-Seq for Illumina Library kit, using the 48 sample protocol on an Apollo 324 liquid handling robot in the Harvard University Bauer Core Facilities. Final library concentration and integrity were again assessed using the QUbit and TapeStation protocols.

Samples intended for transcriptome assembly were sequenced on an Illumina HiSeq 2500, using the standard version 4 protocol, at 125 base pairs of paired-end reads. Samples intended for tissue-specific expression analyses were sequenced on an Illumina NextSeq 500, using a high output flow cell, at 75 base pairs of single-end reads. A table of total read counts for each library can be found in Tables S3-S4. To account for any possible batch effects across separate rounds of sequencing, each sequencing run was performed with one or several overlapping samples. Principle component analysis of these libraries showed variation between sequencing runs to be negligible relative to variation between tissue and individual (see Results and Fig. S7).

3.5 Transcriptome assembling and expression mapping

Transcriptome assembly and expression mapping was performed using the agalma pipeline, version 2.0.0[55]. For the twelve reference transcriptomes, reads from separate rounds of sequencing were concatenated and inserted into the agalma catalog. Further details of transcriptome assembly and homology assessment are included in our previous manuscript[44].

Each tissue-specific expression library was mapped to the corresponding reference transcriptome using the 'expression' pipeline in agalma, which uses the software RSEM to estimate gene and isoform count levels from RNAseq data[56]. The agalma pipeline also includes steps to catalog the species, tissue type, and run information, which were exported as a single JavaScript object notation (JSON) file. This file is available in the GitHub repository in the directory `analysis/data`.

3.6 Phylogenetic analysis

The phylogenetic methods for inferring homology, orthology, and estimating gene and species trees are the same as those described in our previous manuscript[44]. Genetrees were additionally annotated with the software Phyldog[57].

3.7 Annotating transcripts by sequence similarity

We leveraged the close relationship of these species to species of *Drosophila* with well-annotated genomes to annotate the transcripts considered here. For each transcript in the reference transcriptome, we performed four comparisons of sequence similarity using local BLAST: [1] comparing nucleotide transcript sequences to nucleotide sequences from *D. melanogaster* (blastn), [2] comparing translated nucleotide sequences to protein sequences of *D. melanoagster* (blastx), [3] comparing nucleotide sequences to a database of nucleotide sequences from *D. melanogaster*, *D. virilis*, and *D. grimshawi* (blastx), and [4] comparing translated nucleotide sequences to a database of protein sequences from the same three species (blastn). For downstream analyses,

we prioritized annotations from the second comparison, but we provide all sequence similarity reports in the GitHub repository under the directory `analysis/BLAST`.

To annotate homolog groups as defined by the homology inference step of agalma, we extracted the name and sequence ID from all *D. melanogaster* sequences in the group.

3.8 Normalization and differential gene expression

Transcript count tables were imported into R using the agalmar package, version 0.0.0.9000. Differential gene expression analysis was performed using the package DESeq2, version 1.32.0. For these analyses we used only one sequencing run per library, thereby excluding duplicate sequencing runs. Analyses of differential gene expression were calculated using the default approaches in DESeq2 for estimating size factors, dispersions, and calculating $\log_2$ fold-change and p-values (Fig. S2A). Both individual and tissue were considered in the design formula. Transcripts were considered differentially expressed at a significance threshold of 0.01.

We identified a cohort of core ovary-specific genes by first identifying a parent gene for each transcript using a sequence similarity search against *D. melanogaster* (Fig. S2A). We then identified parent genes that had at least one transcript significantly differentially upregulated in the ovary of more than ten of the twelve species. Because multiple transcripts may match to a single parent-gene, core ovary-specific parent genes may include transcripts that are also not differentially upregulated in the ovary, as long as at least one transcript is for more than ten out of twelve species. This may be the case when transcripts are artificially fragmented during reference transcriptome assembly, or when sequence-similar transcripts have biologically distinct expression levels.

3.9 Comparison of expression to *D. melanogaster*

We compared our differential gene expression results to a reference database of tissue expression from *D. melanogaster*, known as the FlyAtlas2[29]. We downloaded this reference in July of 2021, from http://motif.gla.ac.uk/downloads/FlyAtlas2_21.04.18.sql. This dataset provides data on transcript abundance and tissue enrichment, including for female ovaries. Tissue enrichment is calculated using the same methods as in the FlyAtlas2 web browser, defined as the fragments per kilobase of transcript per million mapped reads (FPKM) for a given tissue divided by that value for the reference tissue (here, female whole body), with a pseudocount of two counts added to empty values to avoid division by zero. We considered a FlyAtlas gene to be enriched in the ovary, comparable to our data, if the ovary was the maximum enrichment value across all tissues excluding the head, brain, and eye tissues, as these were separated in our RNASeq procedure (Fig. S2A). We considered a FlyAtlas gene to be head enriched if either the head, brain, or eye were the maximum enrichment value, excluding the ovary.

3.10 Transforming data into comparable measurements of expression across species

Transcript counts are reported in transcripts per million (TPM), but this measurement is known to not be directly comparable across species due to differences in reference transcriptome size[7,8]. Therefore, we normalized TPM by species using the procedure described by Munro and colleagues (2021)[8], where TPM values are multiplied by the number of genes in the reference, and this value is divided by 10^4 (Fig. S2B). TPM10k values were natural-log transformed.

An additional challenge when working with reference transcriptomes is the presence of fragmented transcripts created during the assembly process[58]. This fragmentation can result in noise in estimating the amount of transcript as reads are differentially mapped to these fragments. To reduce the impact of this noise on our analysis, we undertook a novel approach where transcripts were grouped according to inferred homology as estimated by the agalma pipeline using an all-by-all BLAST approach (Fig. S2B). For each sequenced library, we then found the average count value across all transcripts from the same homology group (see

Table S5 for statistics on homology group composition). For each species-tissue pair, we then averaged this value across all biological replicates, here replicate individuals.

3.11 Linear modeling

We performed linear modeling to calculate the relative contribution of tissue- and species-level differences to variation in gene expression (Fig. S2B), following the approach of Breschi and colleagues (2016)[21]. These analyses were performed separately on datasets of ovary vs. carcass and head vs. carcass expression. Using the ANOVA script provided at `https://github.com/abreschi/Rscripts/blob/master/anova.R`, we built a linear model for each gene that accounts for the contribution of the organ, species, and any residual error. We then calculated the relative proportion of each factor divided by the total sum of squares for all factors. We identified groups of highly variable genes, using the same metrics defined by Breschi and colleagues (2016)[21], as any gene for which either tissues or species explains at least 75% of the variance. Species variable genes (SVGs) were defined as highly variable genes whose relative variation was two-fold greater across species than tissues (vice-versa for tissue variable genes, TVGs).

We performed these linear model analyses over four nested clades: a clade containing two *picture-wing* species (*D. sproati* and *D. macrothrix*); a clade containing the four *picture-wing-Nudidrosophila-Ateledrosophila* species in this study; a clade containing the nine Hawaiian *Drosophila* species in this study; and a clade of all 12 Hawaiian *Drosophila* and *Scaptomyza* species in this study. We repeated these analyses excluding the species *S. varia*, which showed the lowest similarity in expression to the other eleven species. To compare our analysis to the more typical approach undertaken, we also performed these analyses on all pairwise combinations of these twelve species.

3.12 Reconstructing evolutionary history of differential expression

We calculated tissue bias as the ratio of counts in TPM10k for each tissue (ovary and head) to the reference tissue[7], here the carcass (Fig. S3A). We subsequently performed the same transformation steps described above, averaging over ratios from the same homology group and across biological replicates, to calculate average expression bias per homology group per library. To avoid division by zero, we added a pseudocount of 0.01 to each TPM10k value. Ratio values were natural-log transformed so that positive values indicate enrichment in the tissue of interest relative to the reference tissue, negative values indicate the opposite, and values of zero indicate equivalent expression.

We reconstructed the evolutionary history of tissue bias for each homology group using the species tree published in Church and Extavour, 2021[44], based on the same reference transcriptome data (Fig. S2C). First, we calibrated the tree estimated using IQtree (Fig 1A of that publication) to be ultrametric using the R function `chronos` in the package `ape`, version 5.5 (using a correlated model and a lambda value of 1). We then subset this tree to only include tips for which expression data was available, and annotated this tree to be able to identify specific branches and nodes in ancestral state reconstruction analyses.

Ancestral expression bias values were estimated with the R package Rphylopars, version 0.3.2, using the fast ancestral state reconstruction algorithm based on Ho and Ané, 2014[59] (Fig. S3A). Tips for which expression data were not available were dropped from each reconstruction, and ancestral state reconstruction was only performed when more than 3 tips had data. Following ancestral state reconstruction, we calculated the scaled change as the difference between the value at the ancestral and descendant nodes, divided by the length of the branch. Scaled changes were compared between homology groups by identifying equivalent branches as those that share the same parent and child node, following the procedure described in Munro and colleagues (2021)[8]. We identified qualitative changes in expression bias as changes that resulted in a ratio changing from negative to positive values or vice versa.

3.13 Estimating correlated evolution of expression across genes

For each homology group that had representation across all twelve species, we calculated pairwise Pearson's correlation coefficients by comparing scaled changes in expression bias across equivalent branches (Fig. S3B). For the twelve-species phylogeny, this meant each correlation coefficient was calculated using 22 individual data points (branches). This resulted in a correlation matrix of 1,306,449 pairwise comparisons of evolutionary correlation.

We compared this correlation network to data on protein interactions and genetic interactions downloaded from http://flybase.org in July, 2021. These data include pairwise observations of genetic enhancement and suppression interactions between parent genes in *D. melanogaster*. These interactions were matched to pairwise correlation coefficients by identifying the corresponding homology group for each *D. melanogaster* parent gene ID (more than one parent gene may fall into the same homology group).

We tested whether correlation coefficients for known genetic interaction partners were higher than in genes with unknown interactions using two-sample t-tests. In each test we compared the coefficients for either enhancement or suppression interactions to a random sample of 5000 coefficients for which interactions are unknown. We repeated these t-tests 100 times using different random samples, and report the maximum p-value observed. We also compared the distribution of enhancement and suppression interaction coefficients to each other using a single t-test.

Strong correlations for the visualization of co-evolutionary networks were selected using a threshold correlation coefficient of 0.825.

4 Data Availability

All data, results, and code for this manuscript are available at GitHub, under the repository `shchurch/hawaiian_drosophilidae_expression_2021`, commit `67d8e6f`. The code to perform all agalma commands was performed in clean anaconda environment, installed following the instructions at `https://bitbucket.org/caseywdunn/agalma`. All R commands were performed with a fresh install of R, and the session information including all package versions is available in the GitHub repository under the file `r_session_info.txt`. The code to generate all plots as well as the text of this manuscript is available in several R scripts and Rmarkdown files at the same location. The resulting correlation matrix can be interactively visualized and queried at the accompanying data visualization for this paper (https://github.com/shchurch/hawaiian_fly_dataviz_2021).

5 Results

5.1 Differential gene expression reveals a cohort of consistently ovary-specific genes

We observed several patterns in tissue-specific gene expression that are consistent across all twelve species. First, in all species the main axis of variation separated ovary RNA libraries from head and carcass (Fig. S4). In all species this axis accounted for at least 50% of variation, and in several species greater than 70% of variation. To test for possible variation due to different runs on the sequencer, we resequenced several libraries and compared them using principle component analysis. We found variation between sequencing runs to be negligible compared to variation across tissues and individuals (Fig. S7). Second, in all species we observed that there was a larger amount of significantly downregulated transcripts than upregulated in the ovary relative to the carcass (Fig. 2A-B, S5). Across species, we observed an average of 27.7% to be significantly downregulated and 15.5% of transcripts to be significantly upregulated. In contrast, when comparing the head to the carcass, we observed an average of 10% of transcripts to be significantly upregulated and 10.5% to be significantly downregulated (Fig. S6). Therefore the ovary shows a larger number of both upregulated

and downregulated genes relative to the carcass than the head, indicating the ovary has a particularly distinct expression profile. These differences may also reflect variation in the complexity and diversity of functions of the tissues being compared.

We used the results of our differential gene expression analysis within species to test for the existence of a suite of genes that show consistent ovary-specific expression across species. We found a cohort of 131 genes, grouped according to BLAST sequence similarity to *D. melanogaster*, for which at least one transcript was significantly upregulated in the ovaries of more than ten species (Fig. 2C). Transcripts matching these genes made up on average 24.6% of the significantly ovary-upregulated transcripts across species, inidicating that a substantial portion of ovary-specific genes have conserved expression patterns over evolutionary time (17.7%, excluding the species *S. varia* that had the most distinct expression profile of all species).

We then tested the extent to which these core ovary genes correspond to observations in well-studied laboratory *Drosophila* models. To accomplish this, we compared expression across Hawaiian species to reported tissue-specific expression levels from *D. melanogaster*[29]. We found that Hawaiian core ovary-specific genes show nearly universal enrichment in the ovary of *D. melanogaster* as well, as reported in the FlyAtlas2 dataset[29] (Fig. 2D). We likewise observed that genes reported in *D. melanogaster* to have highest enrichment in the ovary largely correspond to genes that are significantly upregulated in the ovaries of Hawaiian species (Fig. S8).

The 131 core ovary genes include several well-known members involved in oogenesis and germline stem cell renewal such as *nanos*[34], *swallow*[35], and *oskar*[60](Fig. 2E). We found only two genes that were identified as Hawaiian core ovary genes that are not reported in the FlyAtlas2 dataset[29] to be enriched in the ovary of *D. melanogaster*: the SET domain binding factor *sbf*, and *Rfx*, which are reported to be enriched in the heart, brain, and other non-reproductive tissues[29].

We used the same approach to identify a core suite of 52 head-specific genes (Fig. S9). There was no overlap between the sets of core head genes and core ovary genes. To test whether the correspondence between expression observations in Hawaiian flies and *D. melanogaster* might be due to factors beyond tissue identity, we compared head expression values to ovary enrichment data from *D. melanogaster*, as we had done for ovary expression values above. We did not observe a correspondence in either direction between expression in the head of Hawaiian species and enrichment in the ovary of *D. melanogaster* (Fig. S10A). In contrast, we did find a correspondence between head-specific expression and genes enriched in the *D. melanogaster* brain, eye, and head (Fig. S10B). Core head genes include *Rhodopsin* photoreceptor genes and genes such as *hikaru genki* with involvement in synaptic centers[61].

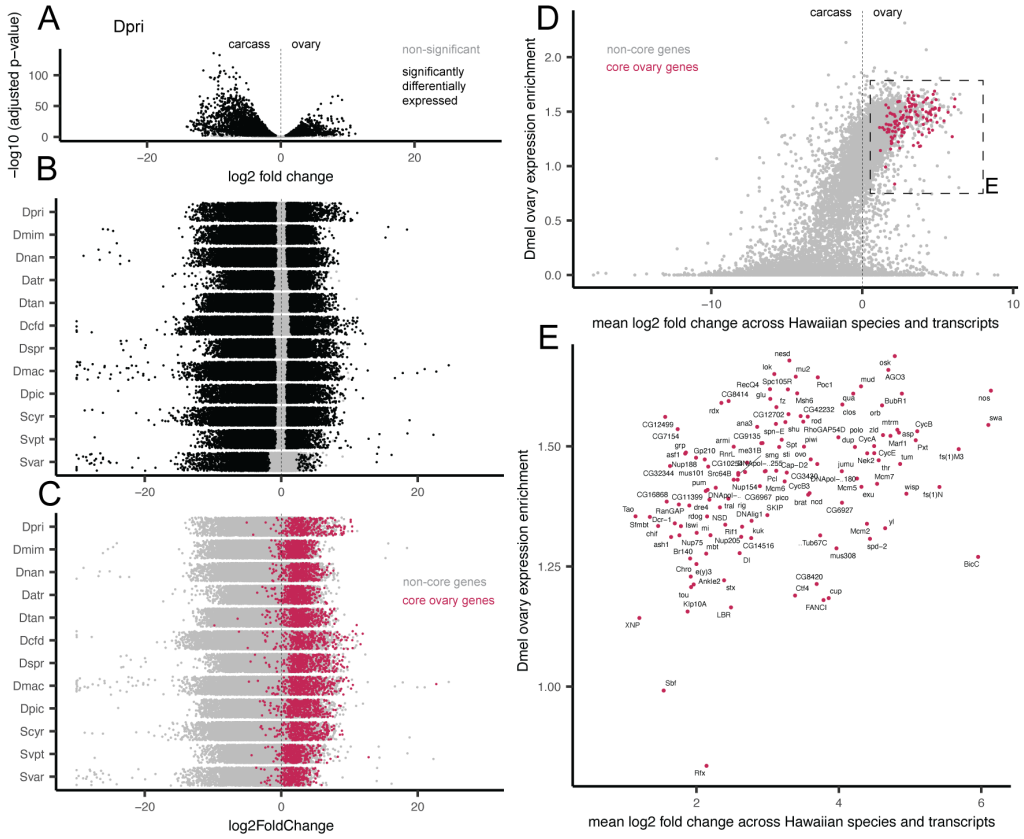

Figure 2: **Identifying a cohort of ovary-specific genes across drosophilid species.** A, Volcano plot for one example species, *D. primaeva* (Dpri), showing the results of a differential gene expression analysis comparing the ovary to the carcass. The x-axis shows the $\log_2$ fold change of expression across transcripts, and the y-axis shows the adjusted p-value, $\log_{10}$ transformed. Points that are significantly differentially expressed are shown in black. B, Jitter plots showing the results of the same analysis across the twelve species studied here. The x-axis shows the $\log_2$ fold change of expression across transcripts, and points are arranged with random jitter within species on the y-axis. C, The same jitter plots, but now colored according to whether or not transcripts belong to a cohort of core ovary genes. These are defined as genes, grouped by BLAST similarity to *D. melanogaster* transcripts, for which at least one transcript is upregulated in the ovary of ten or more of the twelve species. D, A comparison of mean expression change across Hawaiian species to reported ovary-enrichment values from *D. melanogaster*, as reported in FlyAtlas2[29]. Core ovary genes are marked in magenta. E, The same plot, now showing only core ovary genes, annotated with the gene symbol from *D. melanogaster*.

5.2 Modeling reveals the phylogenetic decay of expression similarity between tissues

Many studies have investigated the question of whether we expect expression to be more similar across the same organ in different species, or across different organs within the same species[13–20]. Recent studies have suggested that the answer to this question will depend on the phylogenetic distance separating the species being compared[21]. Here we used a modeling approach to investigate this question with respect to the ovaries of Hawaiian drosophilids.

First, we determined an appropriate unit of comparison across species, based on an assessment of homologous features between reference transcriptomes. The agalma pipeline provides a method for determining

homologous and orthologous sequences using an all-by-all BLAST approach to determine clusters of reciprocally similar sequences (homology groups). These can then be divided into orthology groups by estimating genetrees and identifying maximally inclusive subtrees with no more than one sequence per taxon[55]. We compared the representation of species across homology and orthology groups, and observed that while the representation of homology groups increases with the number of species compared, representation of orthology groups decreases (Fig. S11). This is a known obstacle in comparative transcriptomics, attributed to many transcripts being artifactually fragmented during reference transcriptome assembly[58]. To reduce the impact of this on our downstream analyses, we averaged TPM values across all transcripts within a homology group for each sequenced RNA library. Principle component analysis of this average expression dataset showed that the first principle component divides ovary libraries from the rest, while the second component separates samples along an axis that largely corresponds to phylogenetic distance between species (Fig. S12). While this averaging approach reduces noise due to variable mapping affinities of fragments of the same transcript, it comes at the cost of averaging over potential variation between genuine transcripts that fall into the same homology group. Future analyses using improved assemblies for transcriptomes or genomes will likely be able to avoid this trade off and compare transcript counts directly.

With average expression counts for homologous transcripts across species, we tested the degree to which variation across this dataset could be attributed to tissue-specific variation (here, ovary vs. carcass), species specific variation, or neither (residual variation). Using the linear modeling approach adapted from Breschi and colleagues (2016)[21], we found the proportion of variance across the dataset attributed to tissue differences decreased with phylogenetic distance, while the proportion attributed to species difference increased (Fig. 3A-C). In addition, we found that, when comparing ovary and carcass tissues, the Hawaiian drosophilid clade encompasses the crossover point where variation across species swamps variation across tissues (crossed lines, Fig. 3A). When comparing across the two species from the *picture-wing* group included in this study, an average of 45.6% of the variation can be attributed to tissue differences. For the same comparison, 960 genes were identified as tissue variable genes, defined as residual variation accounting for <25% and a two-fold increase in variation attributed to tissues than to species (Fig. 3B, S13). In contrast, when comparing across all twelve Hawaiian drosophilid species studied here, 34.7% of the variation can be attributed to tissue, with 240 TVGs (Fig. 3B, S13). Across different clades of comparisons, the number of species-variable genes (SVGs) remains relatively stable (from 304 to 260, Fig. 3B).

We then leveraged the results of this linear modeling approach across all twelve species to perform an additional screen for genes that are consistently upregulated in ovaries across species. We compared the proportion of variation explained by tissue for each homology group to the average $\log_2$ fold change from the results of our differential gene expression analysis (Fig 3D). This comparison allowed us to identify genes that fall above our threshold for TVGs that are also upregulated in the ovary (Fig 3E). This group of genes includes many of the same members as the core ovary genes (e.g. *nanos* and *swallow*), as well as several new candidates (e.g. *singed*).

To test the importance of tissue identity, we repeated the same analysis comparing variation across species and tissues using the head in place of the ovary. Consistent with what we describe for the ovary and carcass, as phylogenetic distance increases the proportion of variation across tissues decreases while variation across species increases. In contrast to the above findings, however, for the head and carcass far less of the variation in gene expression can be attributed to tissue differences (Fig. S14). For these tissues, the crossover point between total proportion of variation occurs roughly at the distance separating the two *picture-wing* species.

To verify these results were not driven by the species *S. varia*, which had the most distinct expression patterns of all species, we repeated these analyses excluding this species and recovered largely equivalent results (Fig. S15). To compare our findings to those that would be recovered using a more typical pairwise approach, we repeated the linear modeling analysis on ovary and carcass data using every pairwise combination of the twelve species. We recovered the same trend of decreasing contribution of tissue-level variation with increasing phylogenetic distance, and observed that the variance in mean proportion attributed to either species- or tissue-level differences increased as well (Fig. S16).

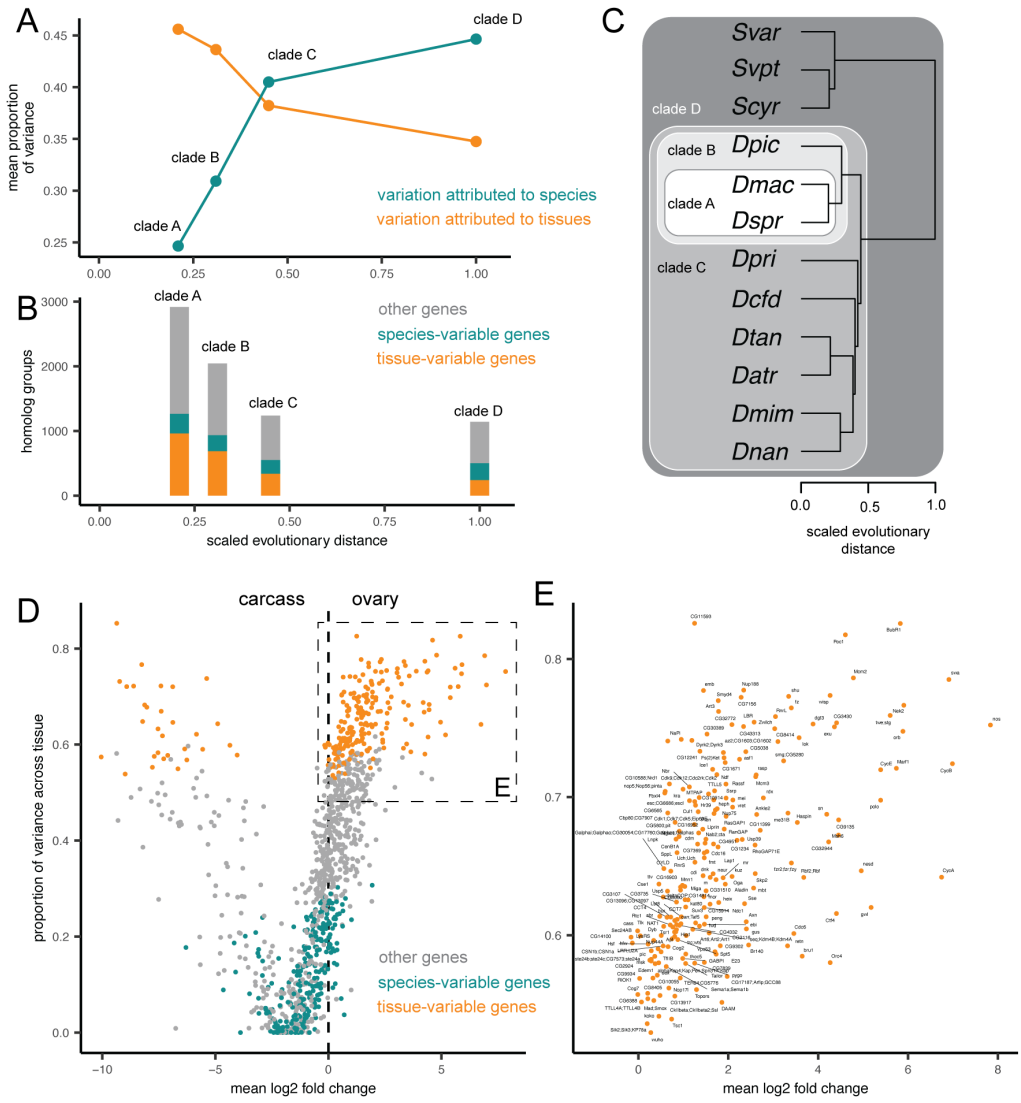

Figure 3: **Linear modeling shows the proportion of variance explained by differences across tissues and species.** A, The results of a linear modeling approach to calculate expression variation for each gene, attributed to variation across organs, species, or residual variation, as described in Breschi and colleagues (2016)[21]. The average proportion of variation attributed to tissues is higher than that attributed to species for the two *picture-wing* species in clade A, while the opposite is true for all twelve species in clade D. B, The number of genes, defined by homology group, classified as tissue variable genes (TVGs), species variable genes (SVGs), or neither in each clade comparison. C, The phylogeny of the twelve species studied here, showing the four clades compared in A-B. Scaled evolutionary distance is calculated as the relative distance from the most recent common ancestor of Hawaiian drosophilids to extant species. D, Comparing results of the differential gene expression approach ($\log_2$ fold change) on the x-axis to results of the modeling approach on the y-axis (variation across tissues). Genes are colored according to TVGs and SVGs. The inset box highlights TVGs that are upregulated in the ovary relative to the carcass. E, The same plot, now showing only upregulated TVGs, annotated with the gene symbol from the *D. melanogaster* sequences in the same homology group.

5.3 Identifying gains and losses of ovary bias across genes and the phylogeny

While a substantial fraction of ovary-specific transcripts belong to the cohort of core ovary genes, on average 75.4% of transcripts are upregulated in the ovaries of one or several species, but not consistently across ten or more of the species studied here (Fig 2B-C). This is suggestive of many evolutionary gains and losses of ovary biased expression of genes. We characterized the evolution of these gains and losses using an ancestral state reconstruction approach. First we quantified expression bias between tissues as the ratio of read counts[7], then reconstructed the value of this continuous trait for each gene (defined using homology groups) at each node of the estimated species tree (Fig. S3). We then calculated the scaled change of expression bias along each branch, which allowed us to describe how relative expression values between tissues had changed the course of evolutionary time (Fig 4A). Visualizing the distribution of scaled changes by genes shows that most scaled changes are small and centered around zero, representing little change in gene expression bias between tissues (Fig. 4B-C).

Using this dataset of scaled changes across genes and branches, we identified branches for which the direction of tissue bias had changed (e.g. from higher expression in the ovary biased than the carcass to lower, or vice versa). Visualizing this dataset according to branches reveals that the majority of these changes in bias are located on the root and terminal branches, rather than internal branches (Fig 4D-E). This is likely because internal branches for this rapid radiation tend to be very short; even when scaling evolutionary changes to branch length, it is less probable to experience a shift to and from ovary biased on a short branch than a long branch. Visualizing the distribution of genes by ancestral and descendant values allows us to identify shifts in bias which represent the largest swings in expression values (Fig. 4F, points a-d). Highlighting the top two such shifts in both directions, we identify four example genes which acquired or lost ovary-specific expression in the phylogeny of Hawaiian Drosophilidae. In the case of *FMRFaR* and *GABA*, a few Hawaiian species have gained ovary biased expression of these genes, while most species and the ancestral state indicate non-ovary bias (Fig. 4Fa-b). In the case of *vilya* and the unnamed gene *CG9109*, each shows a pattern where one species has lost ovary bias from a biased ancestral state (Fig. 4Fc-d).

Repeating the same analysis using the head in place of the ovary revealed a set of evolutionary gains and losses in head-specific expression (Fig. S17). Identifying the top four changes in head expression shows gains and losses of head expression in the genes *hiro*, *stil*, *Jhe*, and, consistent with the ovary, *vilya*. In the case of the latter, these results may be driven by substantial changes in expression of *vilya* in carcass tissues across species, resulting in major differences in both ovary and head-biased expression.

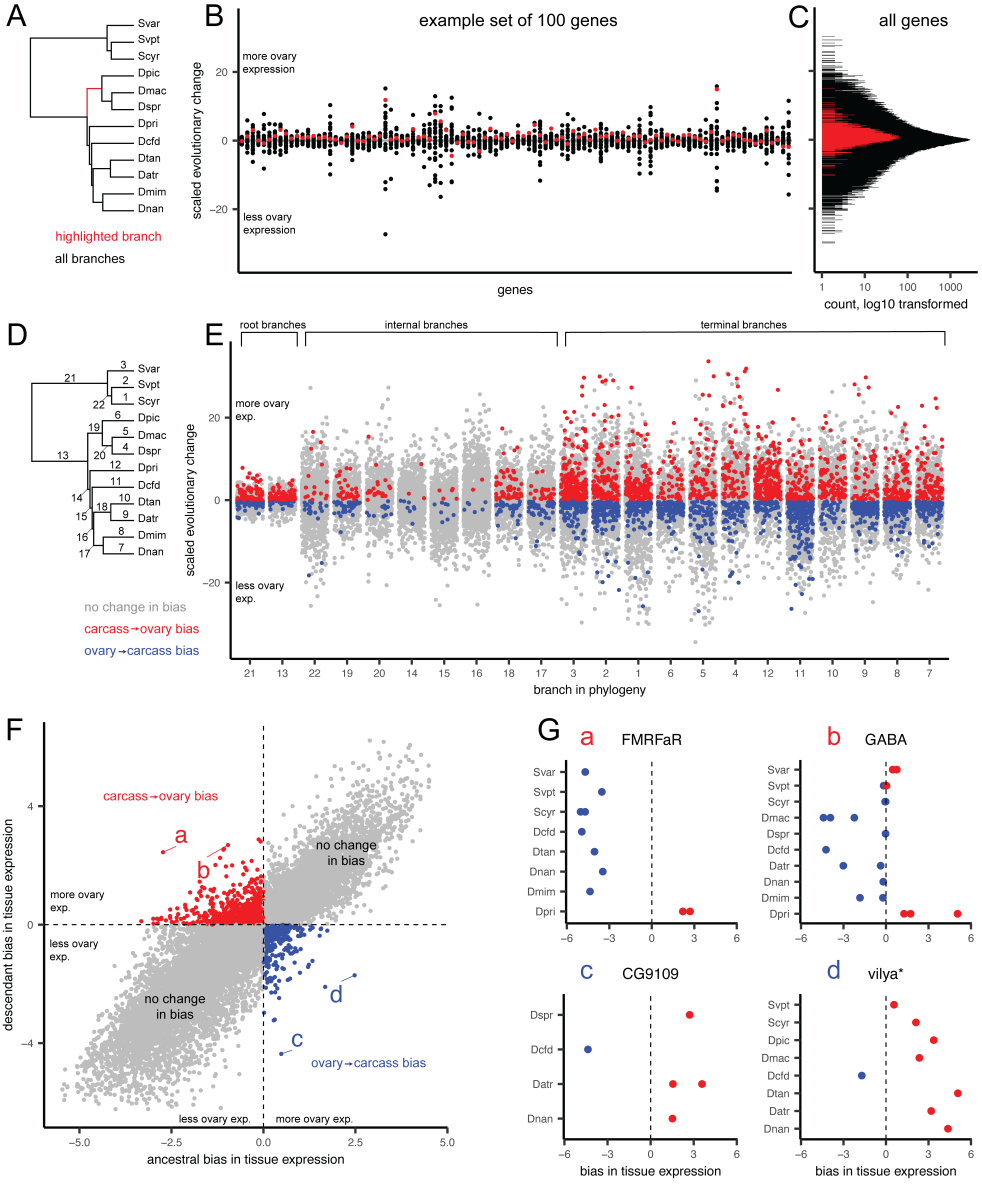

Figure 4: **Identifying genes that have gained and lost ovary expression across the phylogeny.** A, The phylogeny of the twelve species studied here, highlighting one example branch of the 22 for which we inferred the scaled evolutionary change in expression bias. B, The distribution of changes, grouped by gene, for 100 randomly selected genes, defined by homology group. Each point represents one of the 22 branches from A, with the red point corresponding to the highlighted branch from that panel. C, The distribution, $\log_{10}$ transformed, of scaled genes across all branches and all genes. Changes on the highlighted branch in red. D, The phylogeny with all 22 branches numbered. E, The distribution of changes, grouped by branch, with random jitter on the x-axis within each group. Points colored according to the qualitative change in bias, either from more expression in ovary than carcass to less (blue), the reverse (red), or no change in overall bias (gray). F, The distribution of ancestral and descendant values, showing the two quadrants that represent qualitative changes in bias. Points that represent large swings in expression within those quadrants are labeled a-d. G, The four genes with large swings from F, showing the expression bias for each transcript colored according to more expression in the ovary (red) or carcass (blue). Panels annotated with the gene symbol from the *D. melanogaster* sequences in the same homology group, with the exception of *vilya**, which was annotated using a direct BLAST search since no *D. melanogaster* sequence was present in that group.

5.4 Genes with a strong correlation of expression evolution

We tested the estimated evolutionary changes in expression bias for evidence of correlated expression evolution between genes. For every gene represented across all species, we performed a pairwise comparison of changes in expression bias, using as data points the scaled change in ovary bias on the 22 branches in the phylogenetic tree. This resulted in 1,306,449 pairwise measures of evolutionary correlation between genes. Because the number of gene pairs being compared is much larger than the number of values used to estimate correlation, this method has the potential to produce many spurious correlations[7]. To test the degree to which the correlations observed here reflect known biological interactions between genes, we compared these measures to reported protein and genetic interactions between genes, using the database of published genetic experiments in *D. melanogaster*, available at http://flybase.org. We found that the mean correlation coefficient for genes that are known to physically interact as proteins was higher than for genes with no or unknown interaction (p-value=<0.001, Fig. 5A). This indicates that even with a relatively small number of observations, there is sufficient information in the matrix to detect biological signal between gene pairs. These results were calculated based on the correlation in expression bias between the ovary and carcass. However, following the same procedure using correlations in changes in head-biased expression showed no significant difference between the two groups (p-value=0.256, Fig. S18), suggesting the strength of this signal may be dependent on the tissues being compared.

We also found that genes known to interact via genetic enhancement or suppression have a significantly higher mean correlation than genes with no or unknown genetic interactions (unknown vs. enhancement p-value <0.001,unknown vs. suppression=<0.001, Fig. 5B). Comparing genes with known enhancement and suppression interactions to each other showed no significant difference (p-value=0.497). However, for genetic interactions, the range of correlation coefficients was higher in the group of no or unknown interactions (Fig. 5B). This indicates that, while the average correlation of expression evolution might be higher for interaction partners, stronger positive and negative correlations exist between pairs of genes which do not interact, or for which interactions have not yet been tested.

As evidence of this, we compared the interaction network for known ovary-specific genes, to test whether the network inferred based on strong correlation of expression evolution was consistent with known interaction partners from *D. melanogaster*. We selected as an example the gene yolk-protein gene family, which are known to be expressed in the reproductive system, among other tissues[62] (Fig. 5C). We found 8 distinct homologous gene groups, comprising 14 unique *D. melanogaster* parent genes, that had a strong evolutionary correlation with yolk-protein genes (absolute coefficient greater than 0.825, Fig. 5D). None of these correlated genes correspond to those listed on FlyBase[63] as having known interactions with yolk-protein genes in *D. melanogaster* (Fig. 5E). We consider the strong evolutionary correlations to be a set of new predictions about evolutionary and genetic relationships between genes which can be tested in wild and laboratory model species of *Drosophila*. The dataset of pairwise correlation coefficients can be visualized and interrogated at the accompanying data visualization for this manuscript (https://github.com/shchurch/hawaiian_fly_dataviz_2021).

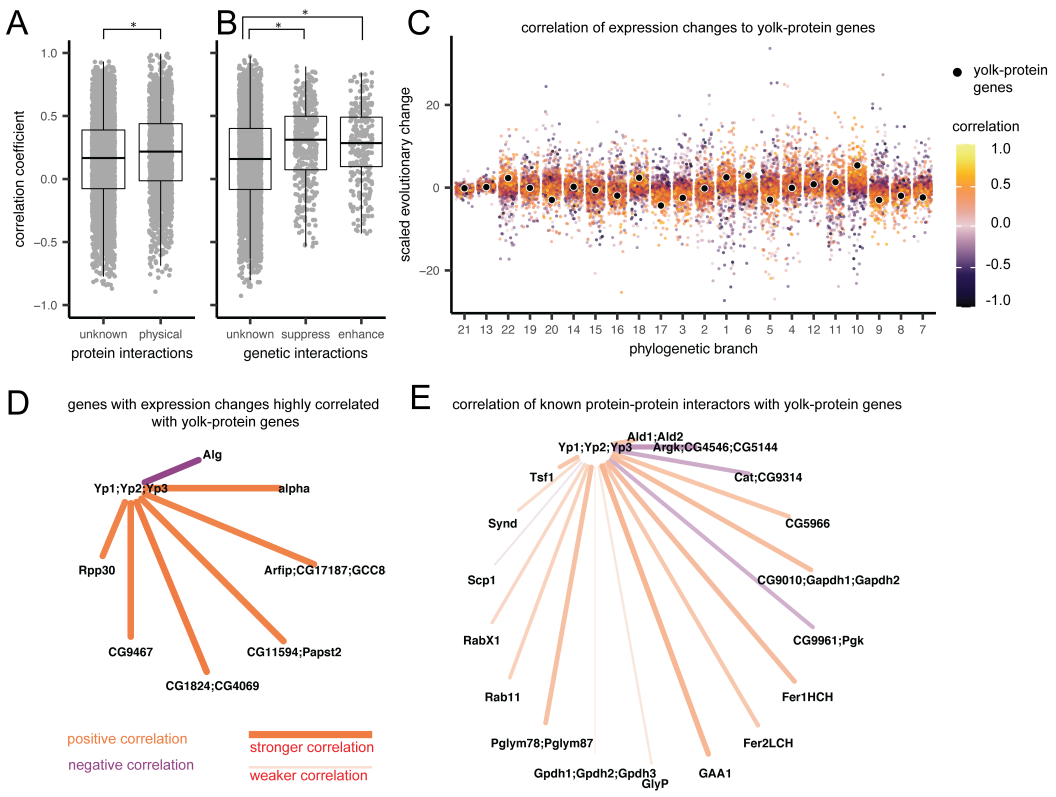

Figure 5: **Estimating pairwise correlation coefficients across genes reveals new networks of correlated expression evolution.** A-B Comparison of the distribution of Pearson's correlation coefficients based on ovary-biased expression evolution between genes. Asterisks indicate a significant t-test comparison. A, Genes with no or unknown protein-protein interactions compared to those with reported interactions in FlyBase[63] (p-value=<0.001). B, Correlation comparison between genes with no or unknown genetic interactions and those reported to have enhancement or suppression interactions in FlyBase (unknown vs. enhancement p-value=<0.001; unknown vs. suppression=<0.001; enhancement vs. suppression=0.497). C, Each point represents a scaled change in expression bias, colored by Pearson's correlation coefficients relative to one example gene-family, the yolk-protein genes (black points), arranged by phylogenetic branch (numbers shown in Fig. 4D). Yellow=strong positive correlation, purple=strong negative correlation. D, The network of strong correlation partners (absolute correlation $>$ 0.825) with the yolk-protein genes, colored by the direction of correlation. Stronger correlations are shown by brighter colors, and thicker, shorter lines. Nodes are annotated with the gene symbols from the *D. melanogaster* sequences from that homology group. E, The correlation between known protein-protein interaction partners[63] with the yolk-protein genes.

6 Discussion

The results of this study show the importance of placing any comparison of gene expression across species in an evolutionary context. When making comparisons that involve model organsism for the study of development and disease, this means identifying the crossover point at which variation between species begins to swamp variation across the tissues or treatments in question. In such comparisons, the possibility that any individual gene may show a divergent pattern of expression from the model organism increases substantially. This study provides evidence that confirms we should expect variation in gene expression to increase with the phylogenetic distance separating the species being compared. In addition, our results using ovary and head expression data show that our expectation should also depend on the identity of the tissues

being compared. Our dataset demonstrates that for some tissues, like the fly head, this crossover point may be met even when comparing between two relatively closely related species.

Despite substantial variation across species, we describe here the composition of core suites of ovary- and head-expressed genes that have maintained conservation of expression patterns over millions of years of evolution. The core ovary genes include some of the most well-studied genes in relation to oogenesis, such as *nanos* and *oskar*, as well as many genes that have yet to be studied in depth (e.g. unnamed genes such as *CG3430*). We provide the full list of core ovary and head genes as a reference against which future genetic studies may be informed and compared (Tables S6-S7). Furthermore, the existence of these suites of genes suggests that equivalent groups are likely to exist within the many gene expression atlases currently being published[64,65]. New technologies such as single-cell RNA sequencing that use global signatures of gene expression to identify cells are ripe for interspecific comparisons that may reveal evolutionary conserved gene modules[66]. Developing robust comparative methods for comparing these atlases across species has the potential to reveal ancestral expression patterns in cells and organs, as well as pinpoint important evolutionary shifts in expression regulation.

Our results indicate that genes known to interact, both physically as proteins and through genetic enhancement and suppression, likely experience more correlated changes in expression than would be expected for genes chosen at random. However, we also find the difference in mean correlation between these groups to be relatively small, and dependent on the context of the tissue in question. One possible explanation for this finding is that interactions between genes with strong correlations of expression evolution have yet to be described. We provide an interactive tool to explore highly correlated genes that can inform future genetic studies in *D. melanogaster* and other related species (https://github.com/shchurch/hawaiian_fly_dataviz_2021). Another possibility we consider likely is that interactions between genes represent one factor among many that dictate the probability of correlated changes in expression. We hypothesize that other features, such as shared regulatory architecture, will also influence evolutionary correlation of expression.

As more studies undertake phylogenetic comparisons of functional genomic data, new factors that influence the evolutionary associations between genes are likely to be revealed[7]. The strength of these phylogenetic comparisons will depend in part on comparing across a sufficient number of taxa such that there are multiple branches on which to calculate and compare evolutionary changes. However, even as functional genomic data become more accessible for more species, the number of features being compared (e.g. thousands of genes) will likely continue to outnumber the number of evolutionary observations (e.g. changes along branches)[7]. One encouraging result from this study is that, using our matrix of gene expression changes along 22 branches, there is sufficient information to detect the biological signal associated with physical and genetic interactions. While this is true, we assume that some fraction of the correlations that we report here represent false positives, and that the strength of correlation of these genes would decrease with the addition of more taxa to the comparison. For this reason we present the correlation matrix as a set of hypotheses to be tested in future studies using additional lines of evidence.

One outstanding challenge in expression evolution is the quality of the references available against which RNA reads can be mapped[58]. In this study we account for the statistical noise in our data by averaging expression values over groups of homologous genes, as identified by sequence similarity to high quality reference genomes. This approach has the advantage of accounting for problems associated with fragmentation of genes in transcriptome assembly. However, it comes at the cost of averaging over possible biological variation in expression between genes from the same gene family. The strong concordance of our results with published records from *D. melanogaster* suggests that the approach we have used here is robust for our dataset. However, as the quality and accessibility of genomes from diverse species continue to increase, future studies will likely be able to compare directly between orthologous genes without needing to account for fragmentation. For those future studies, a phylogenetic comparative approach like the one used here and elsewhere[8] can serve as an analytical framework to move expression comparisons beyond pairwise comparisons.

A goal of evolutionary-developmental biology is to identify changes in developmental mechanisms that underlie phenotypic differences[12]. Many evo-devo studies approach this by identifying phenotypic variation between species and then searching for differences in gene content or expression using one or several emerging model organisms in the lab[12]. To narrow down the field of search, this approach often requires outside knowledge of candidate genes, gained from developmental research in related models or other methods of

filtering the genome. Furthermore, because these approaches usually lack global measurements of gene expression variation across species, identifying an expression difference does not always constitute a smoking gun[6]. For example, observing a difference between candidate gene expression would not be unexpected if we frequently observe differences of that magnitude between genes chosen at random. An alternative approach, as demonstrated here, is to characterize all the evolutionary changes in expression across the transcriptome, and then identify the changes that are significantly associated with traits of interest[9]. As expression data become available from an ever wider array of species, this "evolutionary screen" approach becomes increasingly possible. One advantage of this approach is that it may reveal associations that would otherwise escape detection when comparisons are centered on model organisms; for example, when genes, traits, or processes happen to not be present in our laboratory model species[10]. By leveraging phylogenetic comparative methods on high-dimensional functional genomic data, the objective of connecting genomic variation to developmental mechanisms and phenotypic differences will be accelerated.

References

1. Wang, Z., Gerstein, M. & Snyder, M. RNA-seq: A revolutionary tool for transcriptomics. *Nature Reviews Genetics* **10**, 57–63 (2009).

2. Ozsolak, F. & Milos, P. M. RNA sequencing: Advances, challenges and opportunities. *Nature Reviews Genetics* **12**, 87–98 (2011).

3. Van Dijk, E. L., Auger, H., Jaszczyszyn, Y. & Thermes, C. Ten years of next-generation sequencing technology. *Trends in Genetics* **30**, 418–426 (2014).

4. McDermaid, A., Monier, B., Zhao, J., Liu, B. & Ma, Q. Interpretation of differential gene expression results of RNA-seq data: Review and integration. *Briefings in Bioinformatics* **20**, 2044–2054 (2019).

5. Dunn, C. W., Zapata, F., Munro, C., Siebert, S. & Hejnol, A. Pairwise comparisons across species are problematic when analyzing functional genomic data. *Proceedings of the National Academy of Sciences* **115**, E409–E417 (2018).

6. Church, S. H. & Extavour, C. G. Null hypotheses for developmental evolution. *Development* **147**, dev178004 (2020).

7. Dunn, C. W., Luo, X. & Wu, Z. Phylogenetic analysis of gene expression. *Integrative and Comparative Biology* **53**, 847–856 (2013).

8. Munro, C., Zapata, F., Howison, M., Siebert, S. & Dunn, C. W. Evolution of gene expression across species and specialized zooids in Siphonophora. *bioRxiv* (2021).

9. Smith, S. D., Pennell, M. W., Dunn, C. W. & Edwards, S. V. Phylogenetics is the new genetics (for most of biodiversity). *Trends in Ecology & Evolution* **35**, 415–425 (2020).

10. Dunn, C. W., Leys, S. P. & Haddock, S. H. The hidden biology of sponges and ctenophores. *Trends in Ecology & Evolution* **30**, 282–291 (2015).

11. Arias, A. M. *Drosophila melanogaster* and the development of biology in the 20th century. *Drosophila* **420**, 1–25 (2008).

12. Jenner, R. A. & Wills, M. A. The choice of model organisms in evo–devo. *Nature Reviews Genetics* **8**, 311–314 (2007).

13. Yanai, I., Graur, D. & Ophir, R. Incongruent expression profiles between human and mouse orthologous genes suggest widespread neutral evolution of transcription control. *Omics: a Journal of Integrative Biology* **8**, 15–24 (2004).

14. Lin, S. *et al.* Comparison of the transcriptional landscapes between human and mouse tissues. *Proceedings of the National Academy of Sciences* **111**, 17224–17229 (2014).

15. Gilad, Y. & Mizrahi-Man, O. A reanalysis of mouse ENCODE comparative gene expression data. *F1000Research* **4**, 1–30 (2015).

16. Liao, B.-Y. & Zhang, J. Evolutionary conservation of expression profiles between human and mouse orthologous genes. *Molecular Biology and Evolution* **23**, 530–540 (2006).

17. Cardoso-Moreira, M. *et al.* Gene expression across mammalian organ development. *Nature* **571**, 505–509 (2019).

18. Fukushima, K. & Pollock, D. D. Amalgamated cross-species transcriptomes reveal organ-specific propensity in gene expression evolution. *Nature Communications* **11**, 1–14 (2020).

19. Merkin, J., Russell, C., Chen, P. & Burge, C. B. Evolutionary dynamics of gene and isoform regulation in mammalian tissues. *Science* **338**, 1593–1599 (2012).

20. Brawand, D. *et al.* The evolution of gene expression levels in mammalian organs. *Nature* **478**, 343–348 (2011).

21. Breschi, A. *et al.* Gene-specific patterns of expression variation across organs and species. *Genome Biology* **17**, 1–13 (2016).

22. Robinson, S. W., Herzyk, P., Dow, J. A. & Leader, D. P. FlyAtlas: Database of gene expression in the tissues of *Drosophila melanogaster*. *Nucleic Acids Research* **41**, D744–D750 (2013).

23. Graveley, B. R. *et al.* The developmental transcriptome of *Drosophila melanogaster*. *Nature* **471**, 473–479 (2011).

24. St. Pierre, S. E., Ponting, L., Stefancsik, R., McQuilton, P. & Consortium, F. FlyBase 102—advanced approaches to interrogating flybase. *Nucleic Acids Research* **42**, D780–D788 (2014).

25. Chintapalli, V. R., Wang, J. & Dow, J. A. Using flyatlas to identify better *Drosophila melanogaster* models of human disease. *Nature Genetics* **39**, 715–720 (2007).

26. Papatheodorou, I. *et al.* Expression atlas: Gene and protein expression across multiple studies and organisms. *Nucleic Acids Research* **46**, D246–D251 (2018).

27. Butler, A., Hoffman, P., Smibert, P., Papalexi, E. & Satija, R. Integrating single-cell transcriptomic data across different conditions, technologies, and species. *Nature Biotechnology* **36**, 411–420 (2018).

28. Parisi, M. *et al.* A survey of ovary-, testis-, and soma-biased gene expression in *Drosophila melanogaster* adults. *Genome Biology* **5**, 1–18 (2004).

29. Leader, D. P., Krause, S. A., Pandit, A., Davies, S. A. & Dow, J. A. T. FlyAtlas 2: A new version of the *Drosophila melanogaster* expression atlas with RNA-seq, miRNA-seq and sex-specific data. *Nucleic Acids Research* **46**, D809–D815 (2018).

30. Kumar, T., Blondel, L. & Extavour, C. G. Topology-driven protein-protein interaction network analysis detects genetic sub-networks regulating reproductive capacity. *Elife* **9**, e54082 (2020).

31. Kirilly, D. & Xie, T. The *Drosophila* ovary: An active stem cell community. *Cell Research* **17**, 15–25 (2007).

32. Jagut, M. *et al.* A mosaic genetic screen for genes involved in the early steps of *Drosophila* oogenesis. *G3: Genes, Genomes, Genetics* **3**, 409–425 (2013).

33. Barnett, T., Pachl, C., Gergen, J. P. & Wensink, P. C. The isolation and characterization of *Drosophila* yolk protein genes. *Cell* **21**, 729–738 (1980).

34. Kugler, J.-M. & Lasko, P. Localization, anchoring and translational control of oskar, gurken, bicoid and nanos mRNA during *Drosophila* oogenesis. *Fly* **3**, 15–28 (2009).

35. Stephenson, E. C., Chao, Y.-C. & Fackenthal, J. D. Molecular analysis of the *swallow* gene of *Drosophila melanogaster*. *Genes & development* **2**, 1655–1665 (1988).

36. O'Grady, P. & DeSalle, R. Hawaiian *Drosophila* as an evolutionary model clade: Days of future past. *Bioessays* **40**, 1700246 (2018).

37. Obbard, D. J. *et al.* Estimating divergence dates and substitution rates in the *Drosophila* phylogeny. *Molecular Biology and Evolution* **29**, 3459–3473 (2012).

38. Kambysellis, M. P. *et al.* Pattern of ecological shifts in the diversification of Hawaiian *Drosophila* inferred from a molecular phylogeny. *Current Biology* **5**, 1129–1139 (1995).

39. Montague, J. R., Mangan, R. L. & Starmer, W. T. Reproductive allocation in the Hawaiian Drosophilidae: Egg size and number. *The American Naturalist* **118**, 865–871 (1981).

40. Sarikaya, D. P. *et al.* Reproductive capacity evolves in response to ecology through common changes in cell number in Hawaiian *Drosophila*. *Current Biology* **29**, 1877–1884 (2019).

41. Church, S. H., Donoughe, S., Medeiros, B. A. de & Extavour, C. G. A dataset of egg size and shape from more than 6,700 insect species. *Scientific Data* **6**, 1–11 (2019).

662 42. Church, S. H., Medeiros, B. A. de, Donoughe, S., Márquez Reyes, N. L. & Extavour, C. G. Repeated
663 loss of variation in insect ovary morphology highlights the role of development in life-history evolution.
664 *Proceedings of the Royal Society B* **288**, 20210150 (2021).

665 43. Edwards, K. A., Doescher, L. T., Kaneshiro, K. Y. & Yamamoto, D. A database of wing diversity in the
666 Hawaiian *Drosophila*. *PLoS One* **2**, e487 (2007).

667 44. Church, S. H. & Extavour, C. G. Phylotranscriptomics reveals discordance in the phylogeny of Hawaiian
668 *Drosophila* and *Scaptomyza* (Diptera: Drosophilidae). *bioRxiv* (2021).

669 45. Magnacca, K. N. & Price, D. K. New species of Hawaiian picture wing *Drosophila* (Diptera: Drosophil-
670 idae), with a key to species. *Zootaxa* **3188**, 1–30 (2012).

671 46. Hardy, D. Review of the Hawaiian *Drosophila* (antopocerus) Hardy [insects]. *Proceedings Entomological*
672 *Society of Washington* **79**, 82–95 (1977).

673 47. Hackman, W. On the genus *Scaptomyza* Hardy (Dipt., Drosophilidae) with descriptions of new species
674 from various parts of the world. *Acta Zoologica Fennica* **97**, 1–73 (1959).

675 48. O'Grady, P., Kam, M., Val, F. do & Perreira, W. Revision of the *Drosophila* mimica subgroup, with
676 descriptions of ten new species. *Annals of the Entomological Society of America* **96**, 12–38 (2003).

677 49. Hardy, D. *Diptera: Cyclorrhapha II, Series Schizophora Section Acalypterae I. Family Drosophilidae.*
678 vol. 12 (University of Hawai'i Press, 1965).

679 50. O'Grady, P. M. *et al.* Phylogenetic and ecological relationships of the Hawaiian *Drosophila* inferred by
680 mitochondrial DNA analysis. *Molecular Phylogenetics and Evolution* **58**, 244–256 (2011).

681 51. Lapoint, R. T., Magnacca, K. N. & O'Grady, P. M. Phylogenetics of the Antopocerus-Modified Tarsus
682 clade of Hawaiian *Drosophila*: Diversification across the Hawaiian islands. *PLoS One* **9**, e113227 (2014).

683 52. Katoh, T., Izumitani, H. F., Yamashita, S. & Watada, M. Multiple origins of Hawaiian drosophilids:
684 Phylogeography of *Scaptomyza* hardy (Diptera: Drosophilidae). *Entomological Science* **20**, 33–44 (2017).

685 53. Katoh, K. & Standley, D. M. MAFFT multiple sequence alignment software version 7: Improvements in
686 performance and usability. *Molecular Biology and Evolution* **30**, 772–780 (2013).

687 54. Stamatakis, A. RAxML version 8: A tool for phylogenetic analysis and post-analysis of large phylogenies.
688 *Bioinformatics* **30**, 1312–1313 (2014).

689 55. Dunn, C. W., Howison, M. & Zapata, F. Agalma: An automated phylogenomics workflow. *BMC*
690 *Bioinformatics* **14**, 1–9 (2013).

691 56. Li, B. & Dewey, C. N. RSEM: Accurate transcript quantification from RNA-seq data with or without a
692 reference genome. *BMC Bioinformatics* **12**, 1–16 (2011).

693 57. Boussau, B. *et al.* Genome-scale coestimation of species and gene trees. *Genome Research* **23**, 323–330
694 (2013).

695 58. Freedman, A. H., Clamp, M. & Sackton, T. B. Error, noise and bias in de novo transcriptome assemblies.
696 *Molecular Ecology Resources* **21**, 18–29 (2021).

697 59. Tung Ho, L. si & Ané, C. A linear-time algorithm for gaussian and non-gaussian trait evolution models.
698 *Systematic Biology* **63**, 397–408 (2014).

699 60. McLaughlin, J. M. & Bratu, D. P. *Drosophila melanogaster* oogenesis: An Overview. *Methods in*
700 *molecular biology (Clifton, NJ)* **1328**, 1–20 (2015).

701 61. Hoshino, M., Suzuki, E., Nabeshima, Y.-i. & Hama, C. Hikaru genki protein is secreted into synaptic
702 clefts from an early stage of synapse formation in *Drosophila*. *Development* **122**, 589–597 (1996).

703 62. Garabedian, M. J., Shepherd, B. M. & Wensink, P. C. A tissue-specific transcription enhancer from the
704 *Drosophila* yolk protein 1 gene. *Cell* **45**, 859–867 (1986).

63. Larkin, A. *et al.* FlyBase: Updates to the *Drosophila* melanogaster knowledge base. *Nucleic Acids Research* **49**, D899–D907 (2021).

64. Consortium, T. M. & others. Single-cell transcriptomics of 20 mouse organs creates a *Tabula Muris*. *Nature* **562**, 367–372 (2018).

65. Quake, S. R., Consortium, T. S. & others. The *Tabula Sapiens*: A single cell transcriptomic atlas of multiple organs from individual human donors. *BioRxiv* (2021).

66. Tanay, A. & Sebé-Pedrós, A. Evolutionary cell type mapping with single-cell genomics. *Trends in Genetics* **37**, (2021).

The evolution of ovary-specific gene expression in Hawaiian Drosophilidae: Supplementary methods and tables

Samuel H. Church[1,2,*] Catriona Munro[3] Casey W. Dunn[2]
Cassandra G. Extavour[1,4,5]

Contents

[1] Department of Organismic and Evolutionary Biology, Harvard University, Cambridge, MA 02138, USA

[2] Current address: Department of Ecology and Evolutionary Biology, Yale University, New Haven, CT 06520, USA

[3] Collège de France, PSL Research University, CNRS, Inserm, Center for Interdisciplinary Research in Biology, 75005 Paris, France

[4] Department of Molecular and Cellular Biology, Harvard University, Cambridge, MA 02138, USA

[5] Howard Hughes Medical Institute, Chevy Chase, MD 20815

* corresponding author: samuelhchurch@gmail.com

1 Supplementary figures

1.1 Background

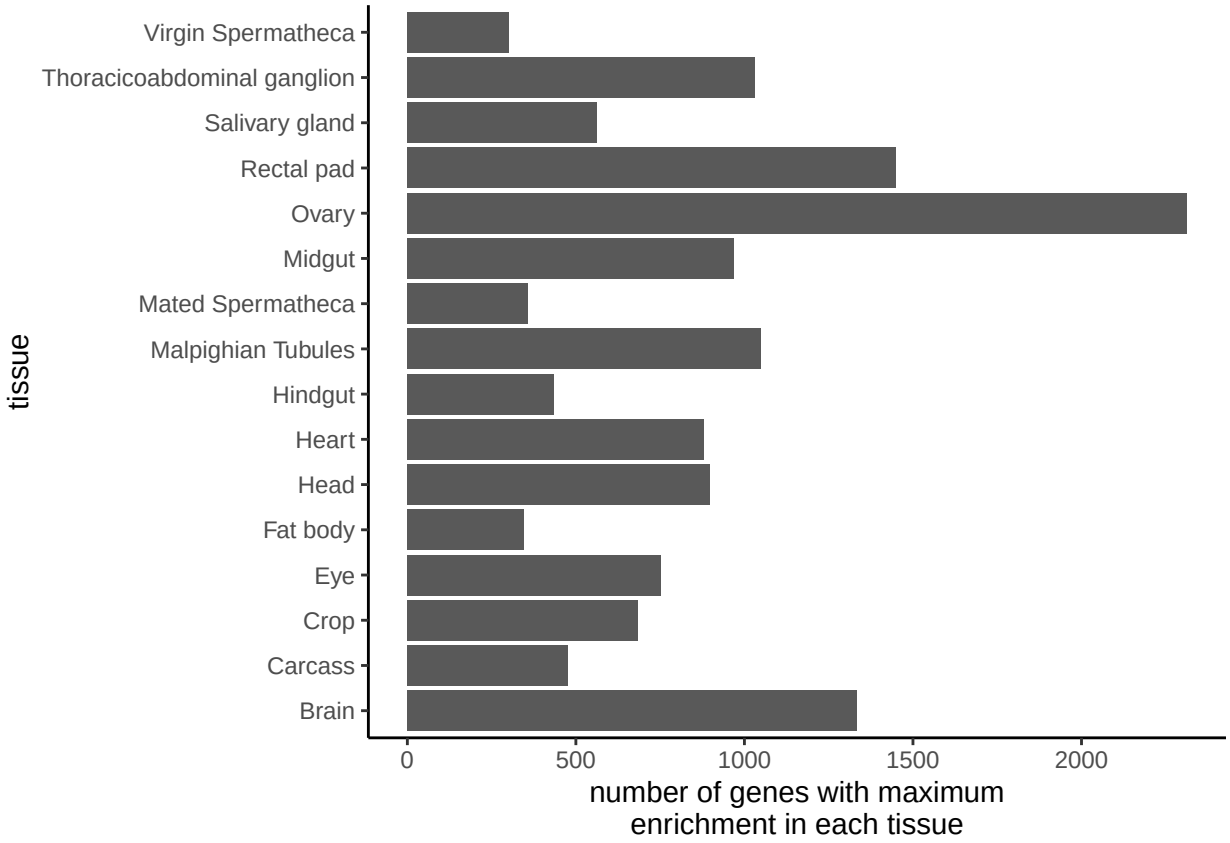

Figure S1: **Comparing across *Drosophila melanogaster* female tissues in the FlyAtlas2 dataset[1], more genes show highest enrichment in the ovary than any other tissue.**

1.2 Analysis pipeline

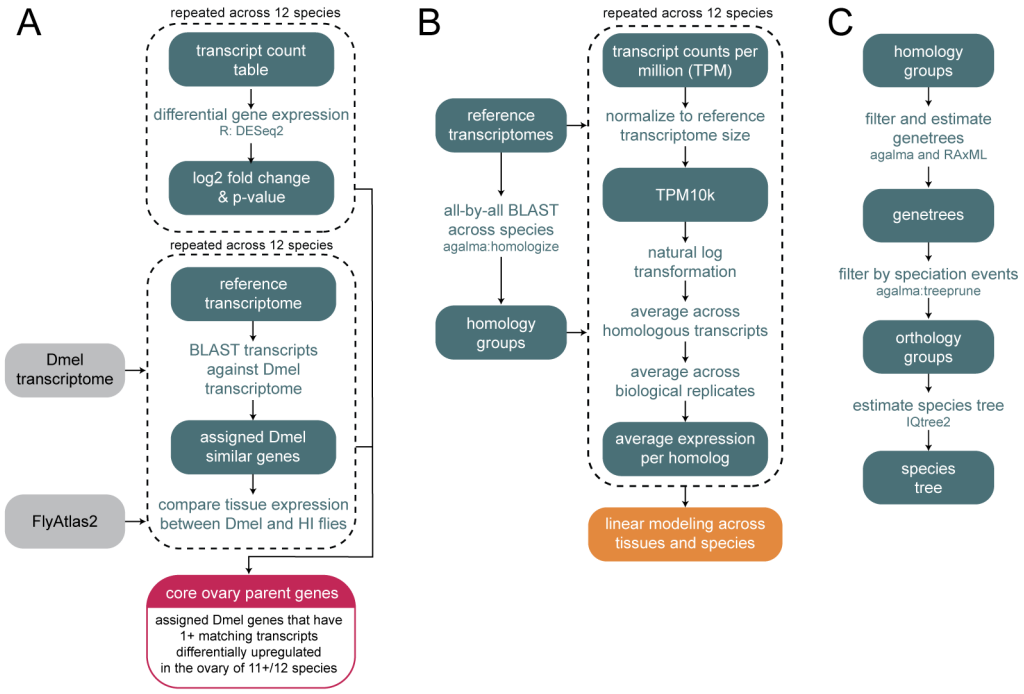

Figure S2: **Analysis pipeline for (A) identifying core ovary genes, (B) linear modeling of expression, and (C) estimating the species level phylogeny. Dmel = *Drosophila melanogster*. HI flies = Hawaiian Drosophilidae.**

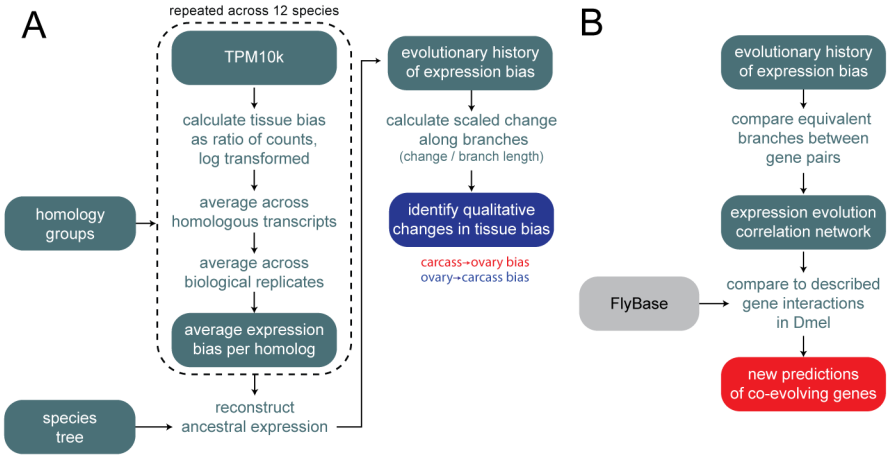

Figure S3: **Analysis pipeline for (A) identifying evolutionary changes in expression bias, and (B) estimating correlation of expression evolution between genes.**

1.3 Differential gene expression

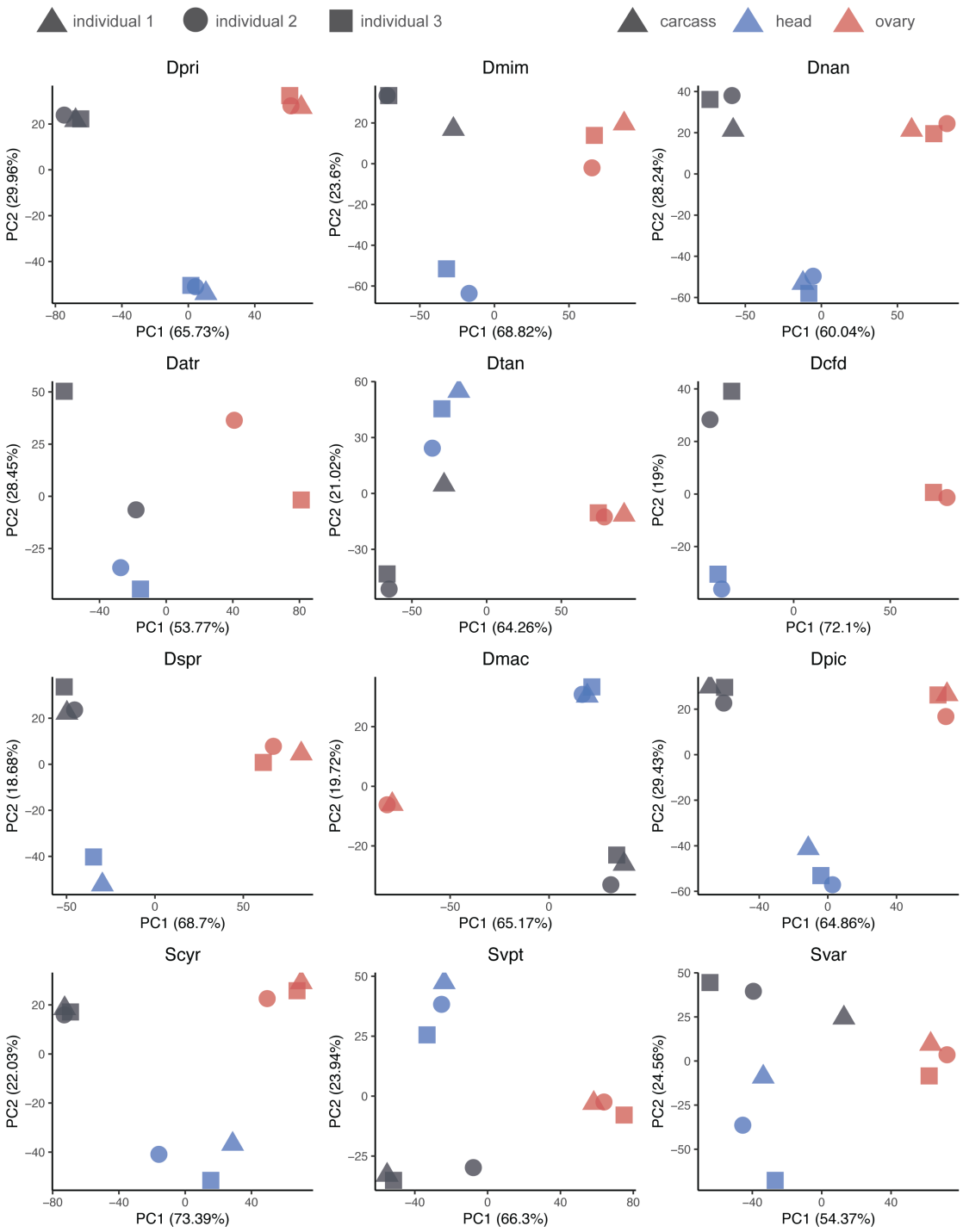

Figure S4: **Principal component analysis within species.** Species abbreviations correspond to names shown in Fig. 1B.

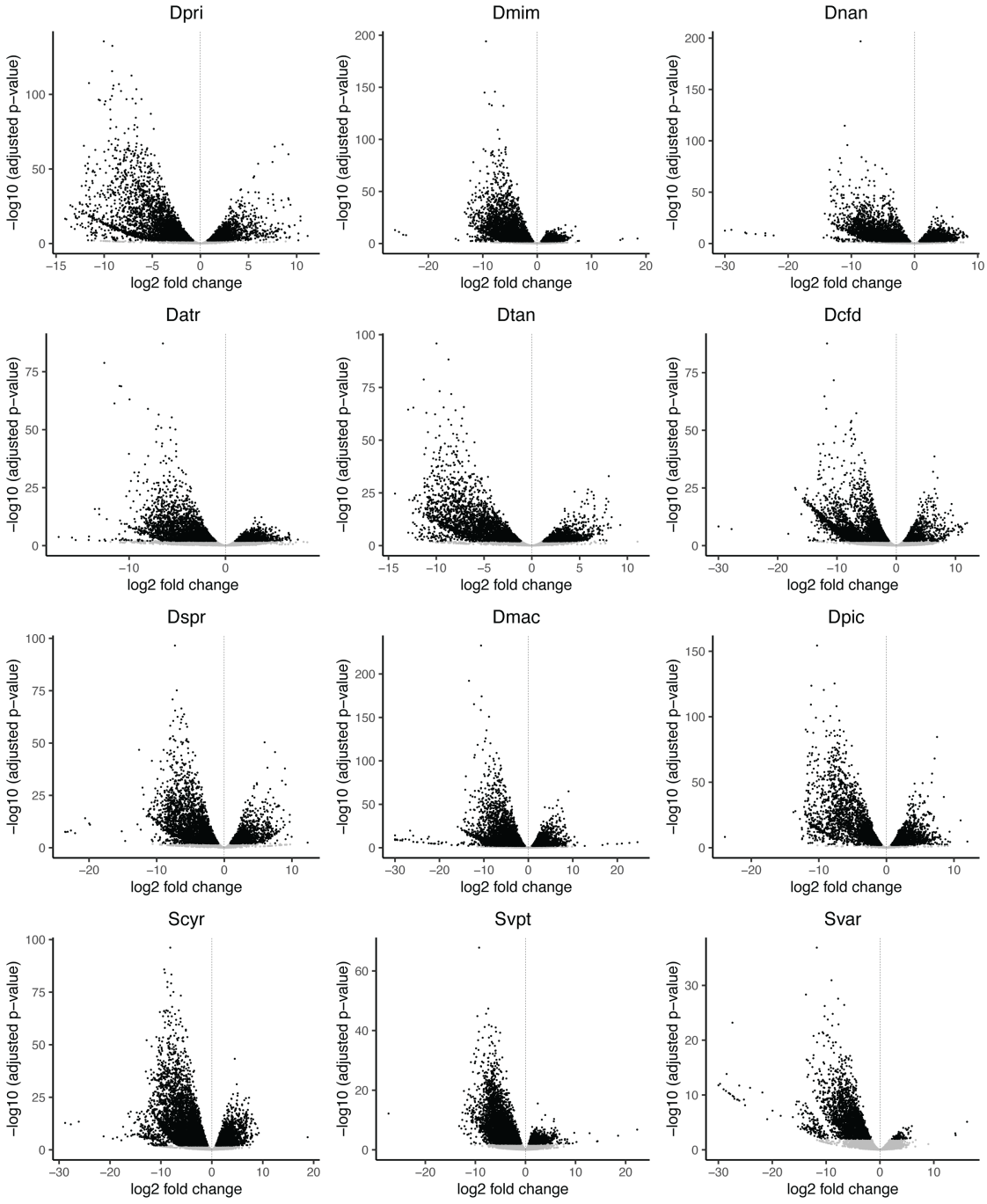

Figure S5: **Differential gene expression volcanos plot comparing ovary and carcass across species.** Species abbreviations correspond to names shown in Fig. 1B. Positive fold changes (points on the right hand side of the volcano) indicate higher expression in the ovary than in the carcass.

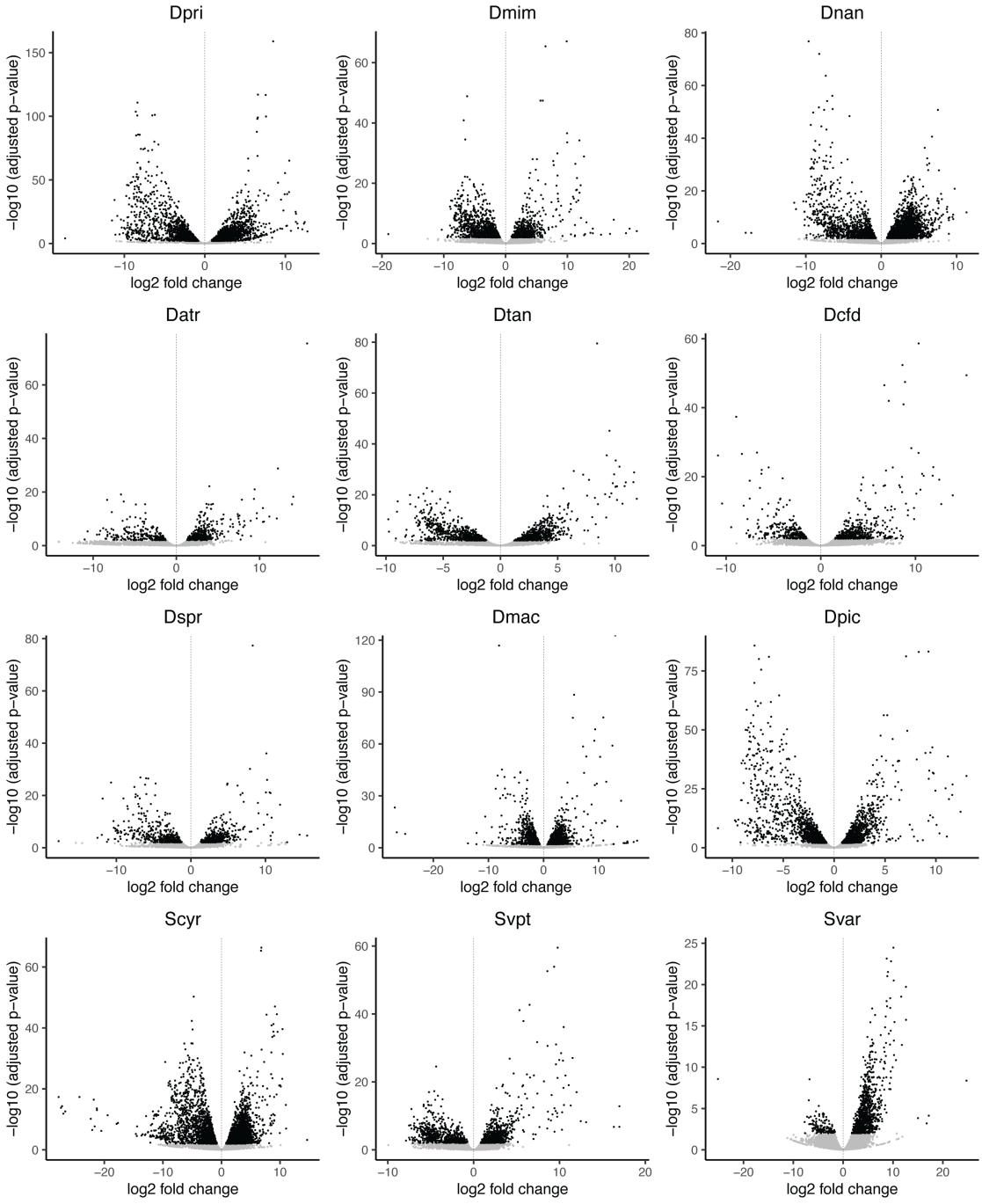

Figure S6: **Differential gene expression volcanos plot comparing head and carcass across species.** Species abbreviations correspond to names shown in Fig. 1B. Positive fold changes (points on the right hand side of the volcano) indicate higher expression in the head than in the carcass.

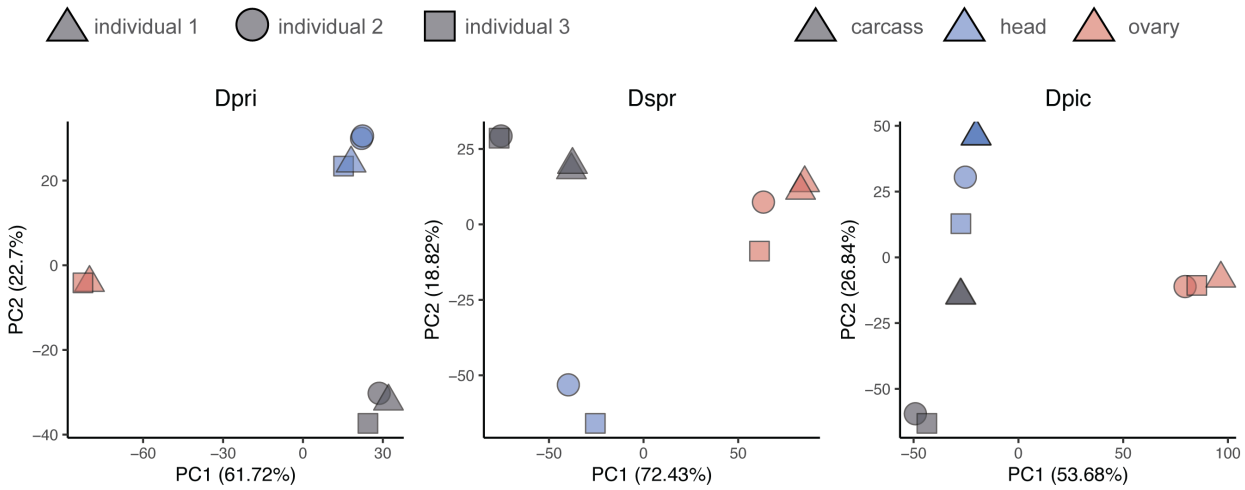

Figure S7: **Principal component analysis showing resequenced libraries.** Species abbreviations correspond to names shown in Fig. 1B.

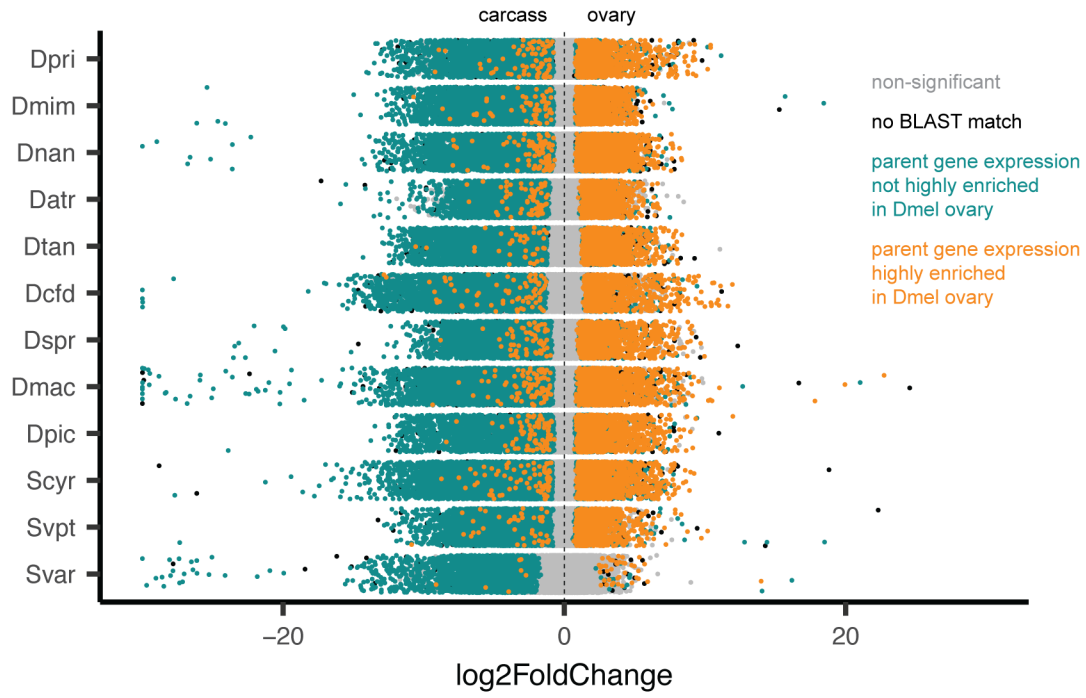

Figure S8: **Differential gene expression analysis across species, colored by *D. melanogaster* expression enrichment.** Points in cyan indicate transcripts that match *D. melanogaster* genes that are not highly enriched in the ovary, according to FlyAtlas2[1]. Orange are transcripts matching genes that are highly enriched in the ovary. Black are transcripts without a BLAST match in *D. melanogaster*. Gray are non-significantly differentially expressed transcripts.

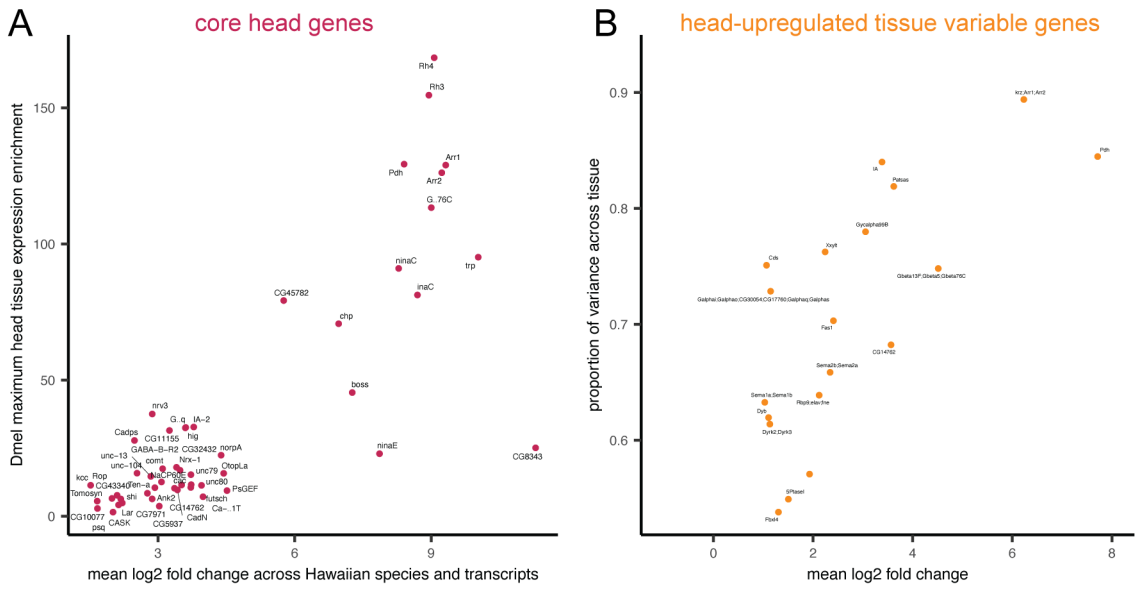

Figure S9: **Differential gene expression analyses comparing head and carcass, colored by *D. melanogaster* expression enrichment.** A, Core head genes, plotted by mean expression change across Hawaiian species to the maximum head, brain, or eye enrichment values from *D. melanogaster*, as reported in FlyAtlas2[1]. Core genes are annotated with the gene symbol from *D. melanogaster*. B, Tissue-variable genes identified in a linear model analysis comparing head and carcass tissues, showing head-upregulated TVGs. Genes are annotated with the gene symbol from the *D. melanogaster* sequences in the same homology group.

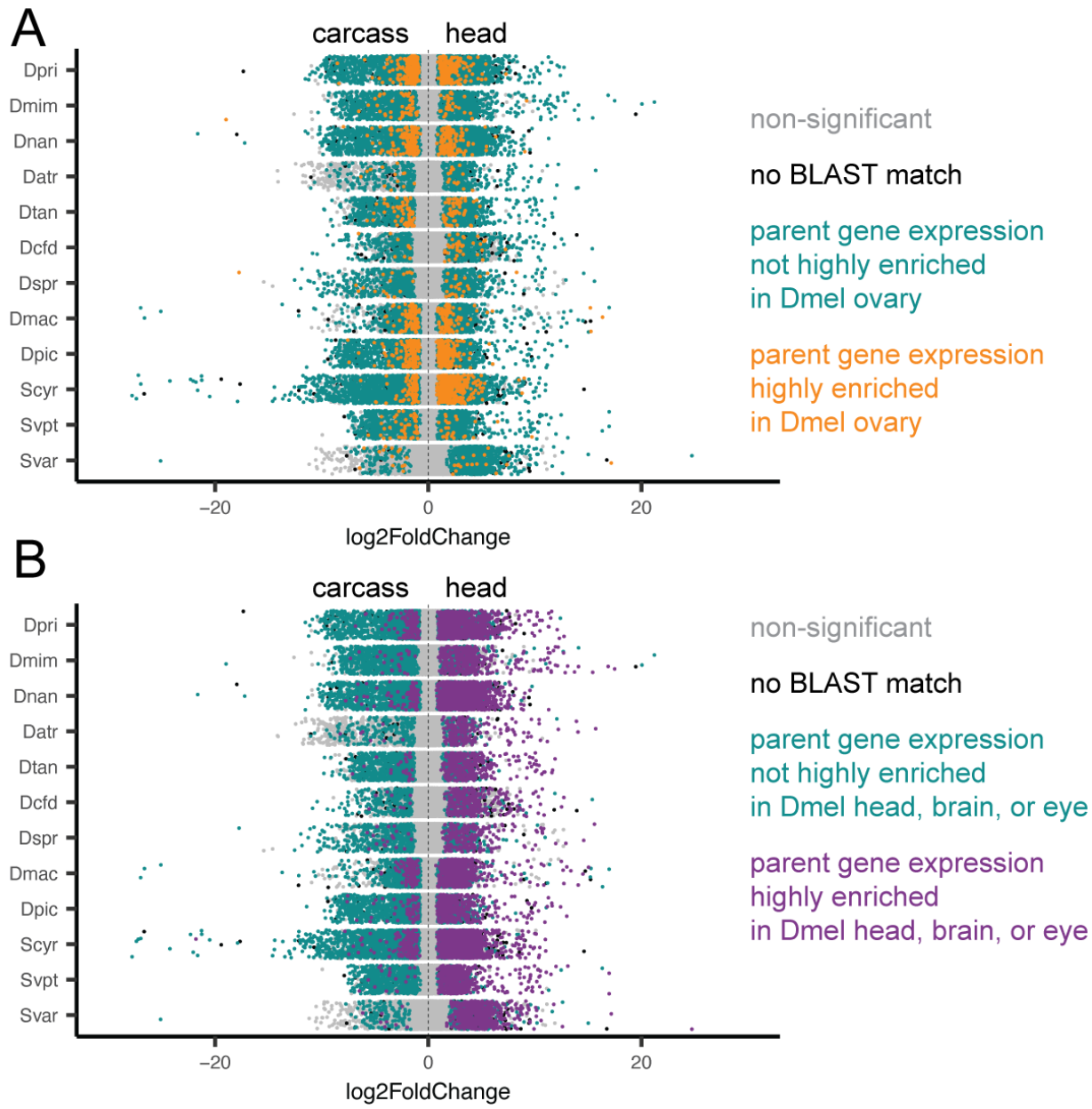

Figure S10: **Differential gene expression analyses comparing head and carcass, colored by *D. melanogaster* expression enrichment.** A, Points in cyan indicate transcripts that match *D. melanogaster* genes that are not highly enriched in the head, according to FlyAtlas2[1]. Orange are transcripts matching genes that are highly enriched in the head. Black are transcripts without a BLAST match in *D. melanogaster*. Gray are non-significantly differentially expressed transcripts. B, The same plot, with purple points as transcripts that are highly enriched in the head, brain, or eye of *D. melanogaster*.

1.4 Linear modeling

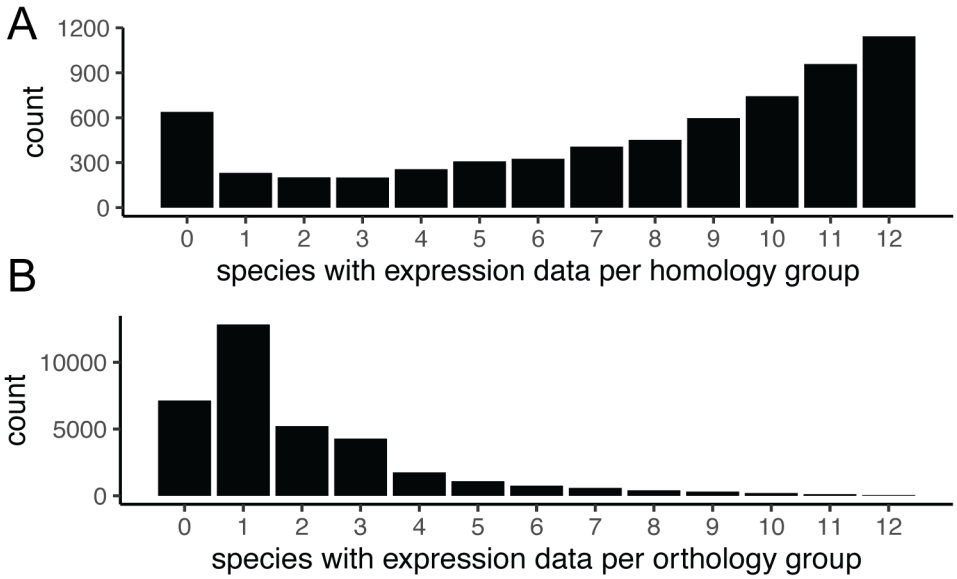

Figure S11: **Representation across homology and orthology groups.** A, The number of species with expression data per homology group, inferred with the agalma pipeline using an all-by-all BLAST approach between the twelve reference transcriptomes and twelve other published Drosophilidae genomes. B, The number of species with expression data per orthology group, inferred with the agalma pipeline, using genetrees to identify orthologs.

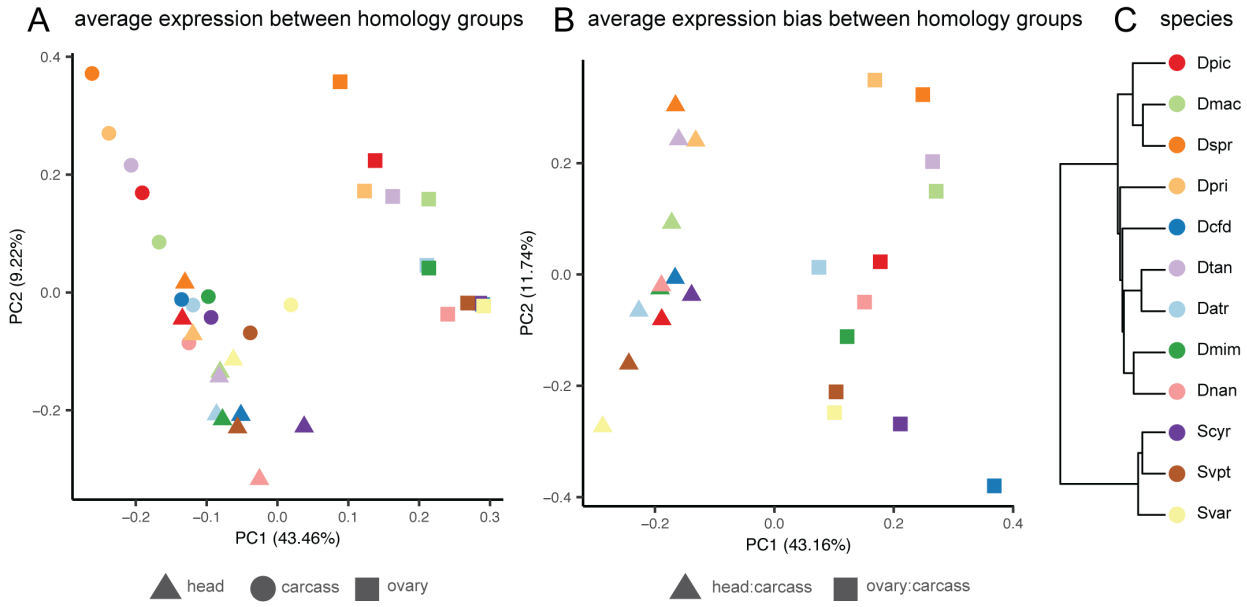

Figure S12: **Principal component analysis across species.** A, PCA using average expression across genes grouped by homology, as inferred with the agalma pipeline. B, PCA using average expression bias, calculated as an expression ratio, across genes grouped by homology. C, Phylogeny of species shown in A and B.

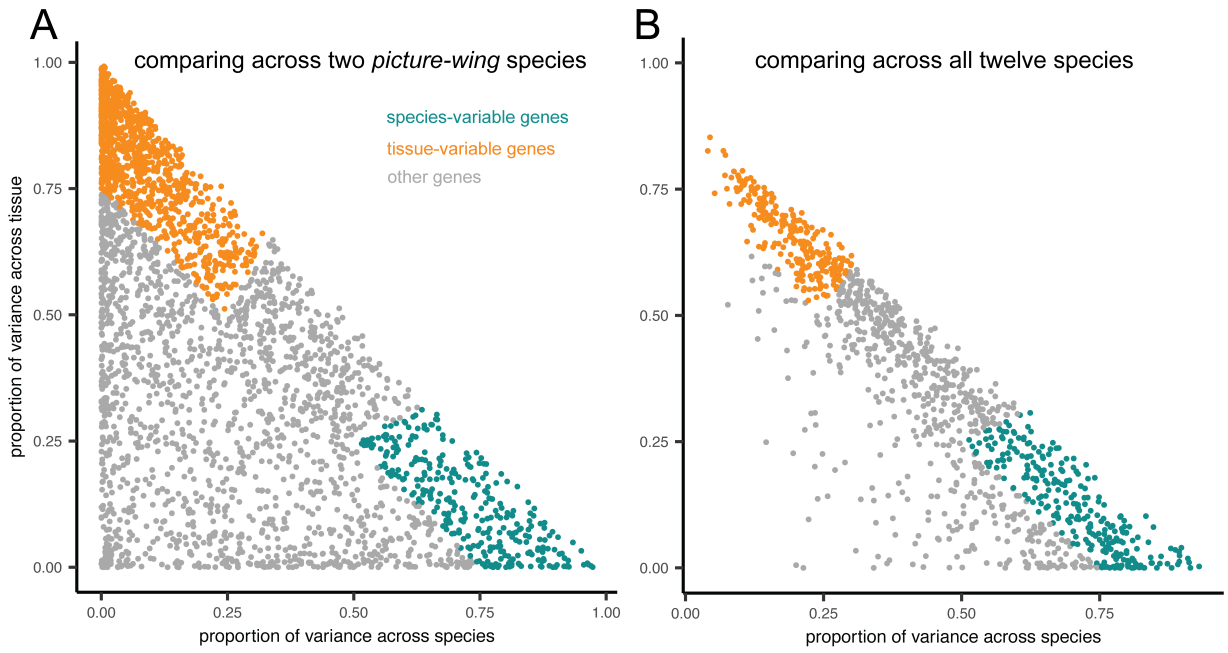

Figure S13: **Linear model results by gene.** A, Results of a linear model analysis between genes, grouped by homology as inferred in the agalma pipeline, comparing two *picture-wing* species, *D. macrothrix* and *D. sproati*. Orange points are tissue-variable genes (TVGs), cyan are species-variable genes (SVGs), gray are neither. B, Results of the same analysis across all twelve Hawaiian drosophilid species studied here.

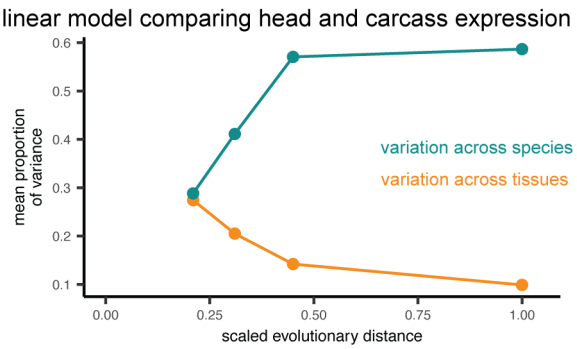

Figure S14: **Proportion of variance across species and tissues, comparing head and carcass.** The mean proportion of variance across genes attributed to species and tissues, comparing the head and carcass across four clades. Clades correspond to those shown in Fig. 3A.

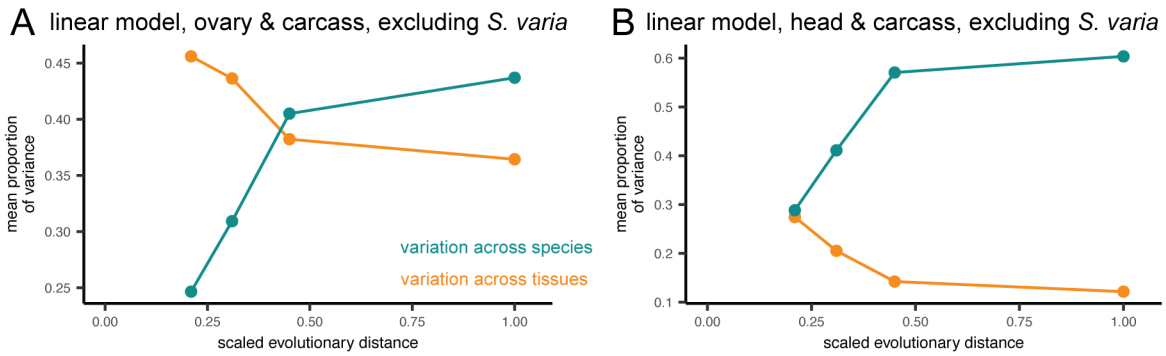

Figure S15: **Proportion of variance across species and tissues, excluding *S. varia*.** A, The mean proportion of variance across genes attributed to species and tissues, comparing the ovary and carcass across four clades, excluding *S. varia* from clade D. B, The same plot, comparing the head and carcass. Clades correspond to those shown in Fig. 3A.

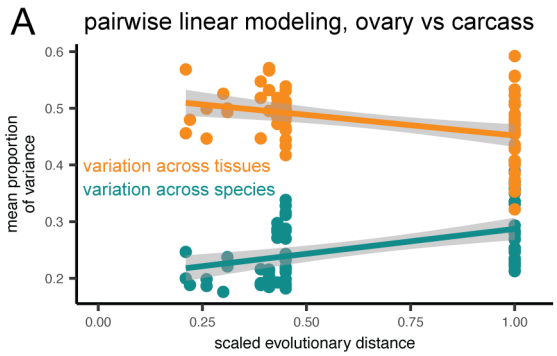

Figure S16: **Proportion of variance across species and tissues, calculated using pairwise combinations of species.** The mean proportion of variance across genes attributed to species and tissues, comparing the ovary and carcass across all pairwise combinations of twelve species. Lines and gray shadow shows the regression and 95% confidence interval using a linear model.

1.5 Phylogenetic analysis

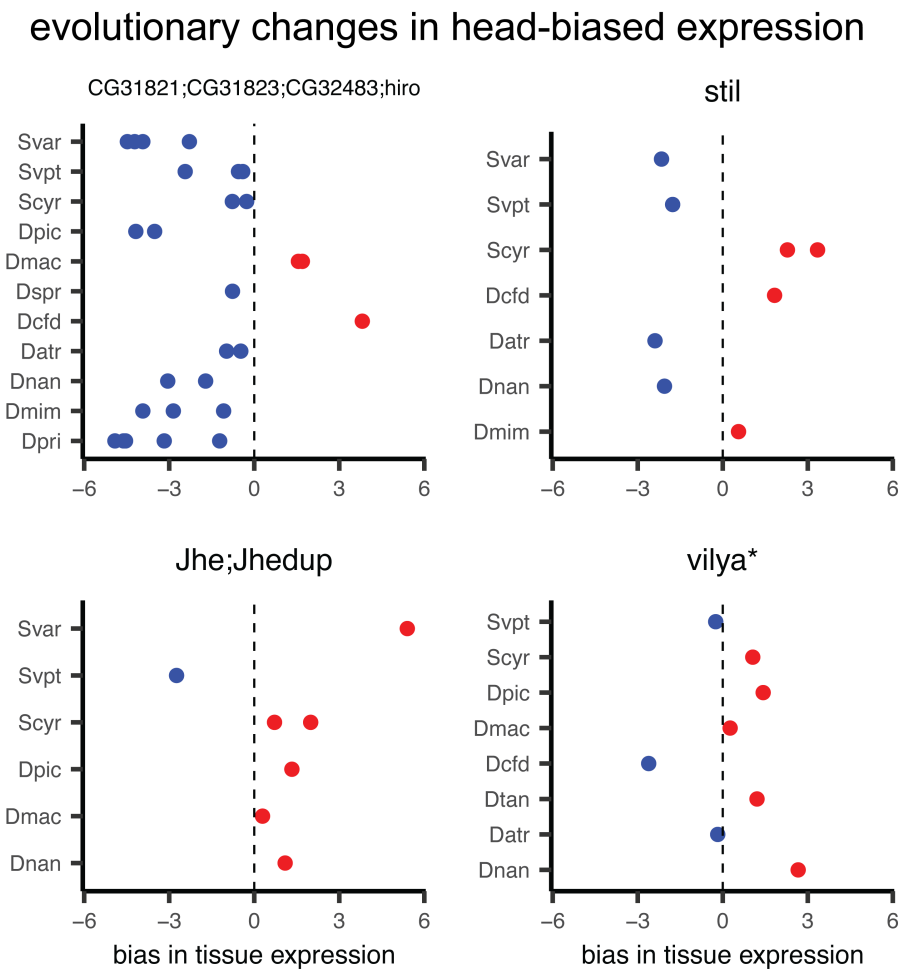

Figure S17: **Changes in head-biased expression evolution.** Four genes displaying large swings in relative head expression, showing the expression bias for each transcript colored according to more expression in the head (red) or carcass (blue). Panels are annotated with the gene symbol from the *D. melanogaster* sequences in the same homology group, with the exception of *vilya**, which was annotated using a direct BLAST search since no *D. melanogaster* sequence was present in that group.

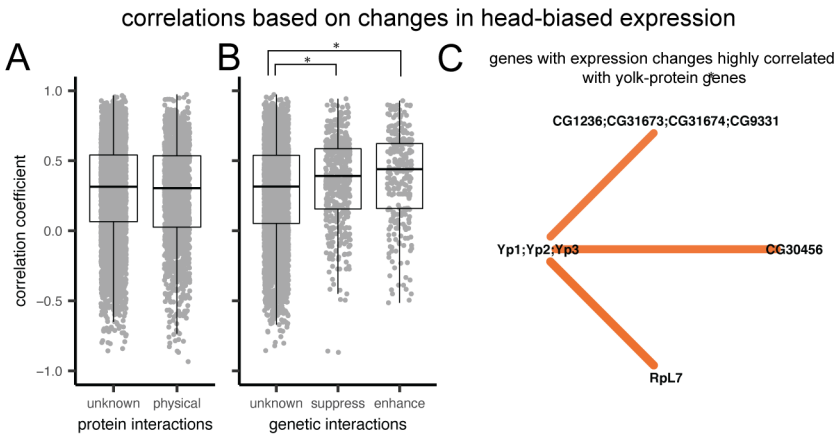

Figure S18: **Evolutionary correlations based on head-biased expression evolution.** A-B Comparison of the dsitribution of Pearson's correlation coefficients based on head-biased expression evolution between genes. Asterisks indicate a significant t-test comparison. A, Genes with no or unknown protein-protein interactions compared to those with reported interactions in FlyBase[2] (p-value=0.256). B, Correlation comparison between genes with no or uknown genetic interactions and those reported to have enhancement or suppression interactions in FlyBase (unknown vs. enhancemenet p-value=<0.001; unknown vs. suppression=<0.001; enhancement vs. suppression=0.248). C, The network of strong correlation partners (absolute correlation > 0.825) with the yolk-protein genes, colored by the direction of correlation. Stronger correlations are shown by brighter colors, and thicker, shorter lines. Nodes are annotated with the gene symbols from the *D. melanogaster* sequences from that homology group.

2 Tables

2.1 Collection and sequencing

Table S1: Field collection information for sequenced specimens.

individual	species	general site	locality	collection method	permit	collection date	GPS
088C	*Scaptomya cyrtandrae*	Stainback Highway	Army road west	on Cyrtandra platyphylla	DOFAW I1012; NARS special use; Hawai'i island forest reserve access permit	5/29/2017	N19° 33.615' W155° 15.010'
088A	*Scaptomya cyrtandrae*	Stainback Highway	Army road west	on Cyrtandra platyphylla	DOFAW I1012; NARS special use; Hawai'i island forest reserve access permit	5/29/2017	N19° 33.615' W155° 15.010'
088B	*Scaptomya cyrtandrae*	Stainback Highway	Army road west	on Cyrtandra platyphylla	DOFAW I1012; NARS special use; Hawai'i island forest reserve access permit	5/29/2017	N19° 33.615' W155° 15.010'
025A	*Drosophila picticornis*	Koke'e State Park	Awa'awapuhi trail	baits	DOFAW I1012; Koke'e state park K2017-2015; I1012; NARS special use; Kaua'i island forest reserves KPI-2017-114	4/14/2017	N22° 08.481' W159° 38.926'
16.2-1	*Drosophila cf dives*	Hawai'i Volcanoes National Park	Bird park	baits	DOFAW I1012; HAVO-2017-SCI-0017	5/10/2016	N19° 26.3512' W155° 18.2225'
16.1-1	*Drosophila cf dives*	Hawai'i Volcanoes National Park	Bird park	baits	DOFAW I1012; HAVO-2017-SCI-0017	5/10/2016	N19° 26.3512' W155° 18.2225'

Table S1: Field collection information for sequenced specimens. *(continued)*

individual	species	general site	locality	collection method	permit	collection date	GPS
18.0-3	*Drosophila mimica*	Hawai'i Volcanoes National Park	Bird park	sweeping Sapindus saponaria leaves	DOFAW I1012; HAVO-2017-SCI-0017	5/10/2016	N19° 26.3512' W155° 18.2225'
040B	*Drosophila mimica*	Hawai'i Volcanoes National Park	Bird park	sweeping Sapindus saponaria leaves	DOFAW I1012; HAVO-2017-SCI-0017	4/17/2017	N19° 26.3512' W155° 18.2225'
040D	*Drosophila mimica*	Hawai'i Volcanoes National Park	Bird park	sweeping Sapindus saponaria leaves	DOFAW I1012; HAVO-2017-SCI-0017	4/17/2017	N19° 26.3512' W155° 18.2225'
040C	*Drosophila mimica*	Hawai'i Volcanoes National Park	Bird park	sweeping Sapindus saponaria leaves	DOFAW I1012; HAVO-2017-SCI-0017	4/17/2017	N19° 26.3512' W155° 18.2225'
032B	*Drosophila nanella*	Koke'e State Park	Drosophila ditch	sweeping Paisonia Leaves	DOFAW I1012; Koke'e state park K2017-2015; I1012; NARS special use; Kaua'i island forest reserves KPI-2017-114	4/16/2017	N22° 04.795' W159° 40.448'
002C	*Drosophila nanella*	Koke'e State Park	Drosophila ditch	sweeping Paisonia Leaves	DOFAW I1012; Koke'e state park K2017-2015; I1012; NARS special use; Kaua'i island forest reserves KPI-2017-114	4/13/2017	N22° 04.795' W159° 40.448'
032A	*Drosophila nanella*	Koke'e State Park	Drosophila ditch	sweeping Paisonia Leaves	DOFAW I1012; Koke'e state park K2017-2015; I1012; NARS special use; Kaua'i island forest reserves KPI-2017-114	4/16/2017	N22° 04.795' W159° 40.448'
002D	*Drosophila nanella*	Koke'e State Park	Drosophila ditch	sweeping Paisonia Leaves	DOFAW I1012; Koke'e state park K2017-2015; I1012; NARS special use; Kaua'i island forest reserves KPI-2017-114	4/13/2017	N22° 04.795' W159° 40.448'
024B	*Drosophila primaeva*	Koke'e State Park	Drosophila gulch	baits	DOFAW I1012; Koke'e state park K2017-2015; I1012; NARS special use; Kaua'i island forest reserves KPI-2017-114	4/16/2017	N22° 08.914' W159° 38.175'
021A	*Drosophila atroscutellata*	Koke'e State Park	Nualolo trail	sweeping Corynocarpus sp leaves	DOFAW I1012; Koke'e state park K2017-2015; I1012; NARS special use; Kaua'i island forest reserves KPI-2017-114	4/15/2017	N22° 07.801' W159° 39.617'
029D	*Drosophila atroscutellata*	Koke'e State Park	Nualolo trail	sweeping Corynocarpus sp leaves	DOFAW I1012; Koke'e state park K2017-2015; I1012; NARS special use; Kaua'i island forest reserves KPI-2017-114	4/16/2017	N22° 07.801' W159° 39.617'
029A	*Drosophila atroscutellata*	Koke'e State Park	Nualolo trail	sweeping Corynocarpus sp leaves	DOFAW I1012; Koke'e state park K2017-2015; I1012; NARS special use; Kaua'i island forest reserves KPI-2017-114	4/16/2017	N22° 07.801' W159° 39.617'
016B	*Drosophila picticornis*	Koke'e State Park	Nualolo trail	baits	DOFAW I1012; Koke'e state park K2017-2015; I1012; NARS special use; Kaua'i island forest reserves KPI-2017-114	4/15/2017	N22° 07.801' W159° 39.617'
016C	*Drosophila picticornis*	Koke'e State Park	Nualolo trail	baits	DOFAW I1012; Koke'e state park K2017-2015; I1012; NARS special use; Kaua'i island forest reserves KPI-2017-114	4/15/2017	N22° 07.801' W159° 39.617'
028A	*Drosophila picticornis*	Koke'e State Park	Nualolo trail	baits	DOFAW I1012; Koke'e state park K2017-2015; I1012; NARS special use; Kaua'i island forest reserves KPI-2017-114	4/15/2017	N22° 07.801' W159° 39.617'
020B	*Scaptomyza varipicta*	Koke'e State Park	Nualolo trail	sweeping Cheirodendron sp leaves	DOFAW I1012; Koke'e state park K2017-2015; I1012; NARS special use; Kaua'i island forest reserves KPI-2017-114	4/15/2017	N22° 08.336' W159° 40.479'

Table S1: Field collection information for sequenced specimens. *(continued)*

individual	species	general site	locality	collection method	permit	collection date	GPS
020C	*Scaptomyza varipicta*	Koke'e State Park	Nualolo trail	sweeping Cheiroden-dron sp leaves	DOFAW I1012; Koke'e state park K2017-2015; I1012; NARS special use; Kaua'i island forest reserves KPI-2017-114	4/15/2017	N22° 08.336' W159° 40.479'
020D	*Scaptomyza varipicta*	Koke'e State Park	Nualolo trail	sweeping Cheiroden-dron sp leaves	DOFAW I1012; Koke'e state park K2017-2015; I1012; NARS special use; Kaua'i island forest reserves KPI-2017-114	4/15/2017	N22° 08.336' W159° 40.479'
020A	*Scaptomyza varipicta*	Koke'e State Park	Nualolo trail	sweeping Cheiroden-dron sp leaves	DOFAW I1012; Koke'e state park K2017-2015; I1012; NARS special use; Kaua'i island forest reserves KPI-2017-114	4/15/2017	N22° 08.336' W159° 40.479'
8.0-1	*Drosophila macrothrix*	Hawai'i Volcanoes National Park	Ola'a tract, pole 44	baits	DOFAW I1012; HAVO-2017-SCI-0017	5/9/2016	N19° 27.722' W155° 14.875'
8.0-2	*Drosophila macrothrix*	Hawai'i Volcanoes National Park	Ola'a tract, pole 44	baits	DOFAW I1012; HAVO-2017-SCI-0017	5/9/2016	N19° 27.722' W155° 14.875'
8.0-3	*Drosophila macrothrix*	Hawai'i Volcanoes National Park	Ola'a tract, pole 44	baits	DOFAW I1012; HAVO-2017-SCI-0017	5/9/2016	N19° 27.722' W155° 14.875'
055A	*Drosophila macrothrix*	Hawai'i Volcanoes National Park	Ola'a tract, pole 44	baits	DOFAW I1012; HAVO-2017-SCI-0017	4/17/2017	N19° 27.722' W155° 14.875'
7.1-1	*Drosophila sproati*	Hawai'i Volcanoes National Park	Ola'a tract, pole 44	baits	DOFAW I1012; HAVO-2017-SCI-0017	5/9/2016	N19° 27.722' W155° 14.875'
7.2-1	*Drosophila sproati*	Hawai'i Volcanoes National Park	Ola'a tract, pole 44	baits	DOFAW I1012; HAVO-2017-SCI-0017	5/9/2016	N19° 27.722' W155° 14.875'
106B	*Drosophila sproati*	Hawai'i Volcanoes National Park	Ola'a tract, pole 44	baits	DOFAW I1012; HAVO-2017-SCI-0017	5/29/2017	N19° 27.722' W155° 14.875'
106A	*Drosophila sproati*	Hawai'i Volcanoes National Park	Ola'a tract, pole 44	baits	DOFAW I1012; HAVO-2017-SCI-0017	5/29/2017	N19° 27.722' W155° 14.875'
043C	*Drosophila tanythrix*	Hawai'i Volcanoes National Park	Ola'a tract, pole 44	baits	DOFAW I1012; HAVO-2017-SCI-0017	4/18/2017	N19° 27.722' W155° 14.875'
056A	*Drosophila tanythrix*	Hawai'i Volcanoes National Park	Ola'a tract, pole 44	baits	DOFAW I1012; HAVO-2017-SCI-0017	4/17/2017	N19° 27.722' W155° 14.875'
40.2-1	*Drosophila tanythrix*	Hawai'i Volcanoes National Park	Ola'a tract, pole 44	baits	DOFAW I1012; HAVO-2017-SCI-0017	5/9/2016	N19° 27.722' W155° 14.875'
043D	*Drosophila tanythrix*	Hawai'i Volcanoes National Park	Ola'a tract, pole 44	baits	DOFAW I1012; HAVO-2017-SCI-0017	4/18/2017	N19° 27.722' W155° 14.875'
008A	*Drosophila primaeva*	Koke'e State Park	Pihea trail	baits	DOFAW I1012; Koke'e state park K2017-2015; I1012; NARS special use; Kaua'i island forest reserves KPI-2017-114	4/14/2017	N22° 08.799' W159° 37.074'
012A	*Drosophila primaeva*	Koke'e State Park	Pihea trail	baits	DOFAW I1012; Koke'e state park K2017-2015; I1012; NARS special use; Kaua'i island forest reserves KPI-2017-114	4/14/2017	N22° 08.799' W159° 37.074'

Table S1: Field collection information for sequenced specimens. *(continued)*

individual	species	general site	locality	collection method	permit	collection date	GPS
008D	*Drosophila primaeva*	Koke'e State Park	Pihea trail	baits	DOFAW I1012; Koke'e state park K2017-2015; I1012; NARS special use; Kaua'i island forest reserves KPI-2017-114	4/14/2017	N22° 08.799' W159° 37.074'
CFC	*Scaptomya varia*	Koke'e State Park	Pihea trail	collected rotting Clermontia sp flowers	DOFAW I1012; Koke'e state park K2017-2015; I1012; NARS special use; Kaua'i island forest reserves KPI-2017-114	4/14/2017	N22° 08.799' W159° 37.074'
CFA	*Scaptomya varia*	Koke'e State Park	Pihea trail	collected rotting Clermontia sp flowers	DOFAW I1012; Koke'e state park K2017-2015; I1012; NARS special use; Kaua'i island forest reserves KPI-2017-114	4/14/2017	N22° 08.799' W159° 37.074'
CFB	*Scaptomya varia*	Koke'e State Park	Pihea trail	collected rotting Clermontia sp flowers	DOFAW I1012; Koke'e state park K2017-2015; I1012; NARS special use; Kaua'i island forest reserves KPI-2017-114	4/14/2017	N22° 08.799' W159° 37.074'

Table S2: DNA barcoding for identification of females.

individual	sample	species match	reference male	external reference sequence	barcode sequence used for final identification	notes
040B	040Bb	*D. mimica*	yes	yes	16S	
040C	040Ctxt	*D. mimica*	yes	yes	16S	
040D	040Db	*D. mimica*	yes	yes	16S	
18.0-3	18.0.17	*D. mimica*	yes	yes	16S	
CFA	CFAb	*S. varia*	yes	yes	COI	
CFB	CFBb	*S. varia*	yes	yes	COI	
CFC	CFCb	*S. varia*	yes	yes	COI	
088A	088Ab	*S. cyrtandrae*	none	yes	COII	
088B	088Bb	*S. cyrtandrae*	none	yes	COII	
088C	088Cb	*S. cyrtandrae*	none	yes	COII	
021A	021Ab	*D. atroscutellata*	yes	yes	COII	
029A	029Atxt	*D. atroscutellata*	yes	yes	COII	
029D	029Db	*D. atroscutellata*	yes	yes	COII	
002C	002Cb	*D. nanella*	yes	yes	16S, COII	
002D	002Dtxt	*D. nanella*	yes	yes	16S, COII	
032A	032Ab	*D. nanella*	yes	yes	16S, COII	
032B	032Bb	*D. nanella*	yes	yes	16S, COII	
106A	106Atxt	*D. sproati*	none	none	COII	matched to other females, morphology is distinctive for females in this species
106B	106Bb	*D. sproati*	none	none	COII	matched to other females, morphology is distinctive for females in this species
7.1-1	7.1.4	*D. sproati*	none	none	COII	matched to other females, morphology is distinctive for females in this species
043C	043Cb	*D. tanythrix*	yes	yes	COII	barcode sequences for D. cognata and D. yooni males suggest hidden complexity in this group
043D	043Dtxt	*D. tanythrix*	yes	yes	COII	barcode sequences for D. cognata and D. yooni males suggest hidden complexity in this group
056A	056Ab	*D. tanythrix*	yes	yes	COII	barcode sequences for D. cognata and D. yooni males suggest hidden complexity in this group
40.2-1	40.2.2	*D. tanythrix*	yes	yes	COII	barcode sequences for D. cognata and D. yooni males suggest hidden complexity in this group
020A	020Atxt	*S. varipicta*	yes	yes	COII	
020B	020Bb	*S. varipicta*	yes	yes	COII	
020C	020Cb	*S. varipicta*	yes	yes	COII	
020D	020Db	*S. varipicta*	yes	yes	COII	

Table S2: DNA barcoding for identification of females. *(continued)*

individual	sample	species match	reference male	external reference sequence	barcode sequence used for final identification	notes
16.1-1	16.1.4	*D. cf dives*	none	none	16S, COII	found no matching reference sequence and no males were caught
16.2-1	16.2.4	*D. cf dives*	none	none	16S, COII	found no matching reference sequence and no males were caught

Table S3: Paired-end sequencing read counts.

species	individual ID	sample ID	tissue	reads - round 1	reads - round 2	reads - round 3	total reads
D. atroscutellata	029A	029Atxt	whole fly	12,520,922	7,801,177	19,925,042	40,247,141
D. cf dives	16.1-1	16.1.1	ovary	16,808,131			16,808,131
D. cf dives	16.1-1	16.1.2	head	18,215,227			18,215,227
D. cf dives	16.1-1	16.1.4	carcass		8,773,601		8,773,601
D. macrothrix	055A	055Atxt	whole fly	10,336,762	10,313,394	19,643,740	40,293,896
D. macrothrix	8.0-2	8.0.6	ovary	8,886,609			8,886,609
D. mimica	040C	040Ctxt	whole fly	9,471,290	8,887,955	15,751,511	34,110,756
D. nanella	002D	002Dtxt	whole fly	10,833,205	7,350,705	17,211,801	35,395,711
D. picticornis	025A	025Atxt	whole fly	10,085,602	10,177,523	16,172,455	36,435,580
D. primaeva	008D	008Dtxt	whole fly	9,129,075	7,583,577	13,937,132	30,649,784
D. sproati	106A	106Atxt	whole fly	7,432,370	6,026,569	10,237,744	23,696,683
D. tanythrix	043D	043Dtxt	whole fly	11,293,054	8,833,878	15,667,639	35,794,571
S. cyrtandrae	088B	088Bb	carcass		9,166,453		9,166,453
S. cyrtandrae	088B	088Bn	head		8,796,864		8,796,864
S. cyrtandrae	088B	088Bo	ovary		9,763,204		9,763,204
S. cyrtandrae	088C	088Cb	carcass	11,218,315			11,218,315
S. cyrtandrae	088C	088Cn	head	7,670,354			7,670,354
S. cyrtandrae	088C	088Co	ovary	7,145,307			7,145,307
S. varia	CFB	CFBb	carcass		6,672,052		6,672,052
S. varia	CFB	CFBn	head		6,311,203		6,311,203
S. varia	CFB	CFBo	ovary		12,672,693		12,672,693
S. varia	CFC	CFCb	carcass	6,941,585			6,941,585
S. varia	CFC	CFCn	head	8,853,906			8,853,906
S. varia	CFC	CFCo	ovary	8,161,304			8,161,304
S. varipicta	020A	020Atxt	whole fly	7,690,349	8,004,757	14,380,332	30,075,438

Table S4: Single-end sequencing read counts.

species	individual ID	sample ID	tissue	notes	reads - round 1	reads - round 2	reads - round 3	reads - round 4	total reads
D. atroscutellata	021A	021Ab	carcass	ovipositor removed			14,147,182		14,147,182
D. atroscutellata	021A	021An	head				14,091,512		14,091,512
D. atroscutellata	021A	021Ao	ovary				17,225,774		17,225,774
D. atroscutellata	029D	029Db	carcass	ovipositor removed				13,664,824	13,664,824
D. atroscutellata	029D	029Dn	head					18,613,630	18,613,630
D. atroscutellata	029D	029Do	ovary	no vitel-logenic eggs				19,916,293	19,916,293
D. cf dives	16.1-1	16.1.1	ovary		12,041,362				12,041,362
D. cf dives	16.1-1	16.1.2	head		18,382,021				18,382,021
D. cf dives	16.1-1	16.1.4	carcass		21,990,829				21,990,829
D. cf dives	16.2-1	16.2.1	ovary		16,508,284				16,508,284
D. cf dives	16.2-1	16.2.2	head			11,288,812			11,288,812
D. cf dives	16.2-1	16.2.4	carcass		14,384,696				14,384,696
D. macrothrix	8.0-1	8.0.1	ovary		625,317	337,147			962,464
D. macrothrix	8.0-1	8.0.2	head		28,027,155	12,695,316			40,722,471
D. macrothrix	8.0-1	8.0.4	carcass		18,125,412				18,125,412
D. macrothrix	8.0-2	8.0.6	ovary		15,583,003				15,583,003
D. macrothrix	8.0-2	8.0.7	head					12,639,355	12,639,355
D. macrothrix	8.0-2	8.0.9	carcass		42,026,251				42,026,251
D. macrothrix	8.0-3	8.0.12	carcass		29,231,317				29,231,317
D. macrothrix	8.0-3	8.0.15	ovary		35,169,909				35,169,909
D. macrothrix	8.0-3	8.0.16	head		17,682,909				17,682,909
D. mimica	040B	040Bb	carcass					13,288,927	13,288,927

Table S4: Single-end sequencing read counts. *(continued)*

species	individual ID	sample ID	tissue	notes	reads - round 1	reads - round 2	reads - round 3	reads - round 4	total reads
D. mimica	040B	040Bn	head					12,473,218	12,473,218
D. mimica	040B	040Bo	ovary					14,622,979	14,622,979
D. mimica	040D	040Db	carcass				20,653,357		20,653,357
D. mimica	040D	040Db	head				12,923,155		12,923,155
D. mimica	040D	040Db	ovary				17,181,968		17,181,968
D. mimica	18.0-3	18.0.14	ovary				13,450,864	17,450,051	30,900,915
D. mimica	18.0-3	18.0.15	head	sequencing failed					0
D. mimica	18.0-3	18.0.17	carcass		19,971,465			11,948,038	31,919,503
D. nanella	002C	002Cb	carcass			15,668,215			15,668,215
D. nanella	002C	002Cn	head			18,850,083			18,850,083
D. nanella	002C	002Co	ovary			19,143,364			19,143,364
D. nanella	032A	032Ab	carcass	ovipositor removed			16,985,268		16,985,268
D. nanella	032A	032An	head				15,262,003		15,262,003
D. nanella	032A	032Ao	ovary				26,566,152		26,566,152
D. nanella	032B	032Bb	carcass	ovipositor removed				13,166,018	13,166,018
D. nanella	032B	032Bn	head					7,720,333	7,720,333
D. nanella	032B	032Bo	ovary					10,507,831	10,507,831
D. picticornis	016B	016Bb	carcass					13,944,238	13,944,238
D. picticornis	016B	016Bn	head					12,710,348	12,710,348
D. picticornis	016B	016Bo	ovary					8,261,788	8,261,788
D. picticornis	016C	016Cb	carcass	ovipositor removed		19,183,647			19,183,647
D. picticornis	016C	016Cn	head			20,597,014			20,597,014
D. picticornis	016C	016Co	ovary			18,242,638			18,242,638
D. picticornis	028A	028Ab	carcass	ovipositor removed			17,704,561	21,917,683	39,622,244
D. picticornis	028A	028An	head				15,060,854	12,034,753	27,095,607
D. picticornis	028A	028Ao	ovary				25,988,121	10,261,716	36,249,837
D. primaeva	008A	008Ab	carcass	ovipositor removed				21,917,683	21,917,683
D. primaeva	008A	008An	head					12,034,753	12,034,753
D. primaeva	008A	008Ao	ovary					10,261,716	10,261,716
D. primaeva	012A	012Ab	carcass			16,297,595			16,297,595
D. primaeva	012A	012An	head			12,515,877			12,515,877
D. primaeva	012A	012Ao	ovary	all oocytes were at the same stage		14,945,335			14,945,335
D. primaeva	024B	024Bb	carcass				21,578,797		21,578,797
D. primaeva	024B	024Bn	head				13,850,246		13,850,246
D. primaeva	024B	024Bo	ovary	all oocytes were at the same stage			12,001,961		12,001,961
D. sproati	106B	106Bb	carcass			17,653,753			17,653,753
D. sproati	106B	106Bn	ovary			10,220,778			10,220,778
D. sproati	106B	106Bo	head			15,615,762			15,615,762
D. sproati	7.1-1	7.1.1	ovary		9,527,229				9,527,229
D. sproati	7.1-1	7.1.2	head	sequencing failed					0
D. sproati	7.1-1	7.1.4	carcass		13,815,824				13,815,824
D. sproati	7.2-1	7.2.1	carcass		22,462,042				22,462,042
D. sproati	7.2-1	7.2.2	head		21,654,908				21,654,908
D. sproati	7.2-1	7.2.4	ovary		31,064,408				31,064,408
D. tanythrix	043C	043Cb	carcass			11,381,085			11,381,085
D. tanythrix	043C	043Cn	head			9,395,340			9,395,340
D. tanythrix	043C	043Co	ovary			13,769,669			13,769,669
D. tanythrix	056A	056Ab	carcass				20,904,414		20,904,414
D. tanythrix	056A	056An	head				13,824,612		13,824,612
D. tanythrix	056A	056Ao	ovary				17,772,798		17,772,798
D. tanythrix	40.2-1	40.2.1	ovary		30,223,622				30,223,622
D. tanythrix	40.2-1	40.2.2	head		27,274,868		17,405,688	17,790,177	62,470,733
D. tanythrix	40.2-1	40.2.4	carcass		22,021,646	16,772,624			38,794,270
S. cyrtandrae	088A	088Ab	carcass			19,038,552			19,038,552
S. cyrtandrae	088A	088An	head			12,179,789			12,179,789
S. cyrtandrae	088A	088Ao	ovary			13,439,568			13,439,568
S. cyrtandrae	088B	088Bb	carcass				11,543,268		11,543,268
S. cyrtandrae	088B	088Bn	head				12,904,077		12,904,077
S. cyrtandrae	088B	088Bo	ovary				11,569,554		11,569,554
S. cyrtandrae	088C	088Cb	carcass					15,301,343	15,301,343
S. cyrtandrae	088C	088Cn	head					8,191,593	8,191,593

Table S4: Single-end sequencing read counts. *(continued)*

species	individual ID	sample ID	tissue	notes	reads - round 1	reads - round 2	reads - round 3	reads - round 4	total reads
S. cyrtandrae	088C	088Co	ovary					7,158,247	7,158,247
S. varia	CFA	CFAb	carcass			14,094,153			14,094,153
S. varia	CFA	CFAn	head			10,655,605			10,655,605
S. varia	CFA	CFAo	ovary			10,702,817			10,702,817
S. varia	CFB	CFBb	carcass				8,049,520		8,049,520
S. varia	CFB	CFBn	head				7,357,905		7,357,905
S. varia	CFB	CFBo	ovary				12,557,066		12,557,066
S. varia	CFC	CFCb	carcass					11,159,366	11,159,366
S. varia	CFC	CFCn	head					11,517,456	11,517,456
S. varia	CFC	CFCo	ovary					10,874,670	10,874,670
S. varipicta	020B	020Bb	carcass			8,132,403			8,132,403
S. varipicta	020B	020Bn	head			14,331,603			14,331,603
S. varipicta	020B	020Bo	ovary			8,192,636			8,192,636
S. varipicta	020C	020Cb	carcass	ovipositor removed			16,584,774		16,584,774
S. varipicta	020C	020Cn	head				13,783,546		13,783,546
S. varipicta	020C	020Co	ovary				17,539,765		17,539,765
S. varipicta	020D	020Db	carcass	ovipositor removed				19,358,586	19,358,586
S. varipicta	020D	020Dn	head					19,832,422	19,832,422
S. varipicta	020D	020Do	ovary					13,226,137	13,226,137

Table S5: Number of transcripts per homology group per species.

species	homology groups	groups with more than one transcript	max num. transcripts per group	ave num. transcripts per group
D. atroscutellata	3,939	1,211	8	1.40
D. cf dives	4,782	966	8	1.28
D. macrothrix	4,061	1,164	8	1.39
D. mimica	4,278	1,344	8	1.42
D. nanella	4,790	1,271	7	1.36
D. picticornis	2,769	784	6	1.37
D. primaeva	3,274	935	7	1.39
D. sproati	3,380	767	8	1.30
D. tanythrix	3,618	1,015	7	1.38
S. cyrtandrae	4,966	1,283	7	1.35
S. varia	4,733	1,109	12	1.32
S. varipicta	4,696	1,195	8	1.35

2.2 Core genes

Table S6: Core ovary genes.

Dmel parent gene ID	Dmel parent gene symbol	transcripts in homology group	homology group Dmel sequence symbols
FBgn0250816	AGO3	none	none
FBgn0087040	alphaTub67C	none	none
FBgn0266111	ana3	none	none
FBgn0028343	Ankle2	some	Ankle2
FBgn0041164	armi	none	none
FBgn0029094	asf1	all	asf1
FBgn0005386	ash1	none	none
FBgn0000140	asp	none	none
FBgn0000182	BicC	none	none
FBgn0033155	Br140	some	Br140
FBgn0010300	brat	some	brat
FBgn0263855	BubR1	some	BubR1
FBgn0039680	Cap	none	none
FBgn0027512	CG10254	none	none
FBgn0037021	CG11399	some	CG11399
FBgn0038968	CG12499	none	none
FBgn0031070	CG12702	none	none
FBgn0039640	CG14516	none	none
FBgn0034498	CG16868	none	none
FBgn0052344	CG32344	none	none
FBgn0031875	CG3430	some	CG3430
FBgn0250754	CG42232	none	none
FBgn0029733	CG6927	some	CG6927;pHCl;SecCl

Table S6: Core ovary genes. *(continued)*

Dmel parent gene ID	Dmel parent gene symbol	transcripts in homology group	homology group Dmel sequence symbols
FBgn0034187	CG6967	some	CG6701;CG6967
FBgn0031947	CG7154	some	CG7154
FBgn0034073	CG8414	all	CG8414
FBgn0037664	CG8420	none	none
FBgn0031769	CG9135	some	CG9135
FBgn0000307	chif	none	none
FBgn0044324	Chro	none	none
FBgn0261016	clos	some	no Dmel match
FBgn0033890	Ctf4	some	Ctf4
FBgn0000392	cup	none	none
FBgn0000404	CycA	some	CycA
FBgn0000405	CycB	some	CycB
FBgn0015625	CycB3	some	CycB3
FBgn0010382	CycE	some	CycE
FBgn0039016	Dcr	some	no Dmel match
FBgn0000463	Dl	none	none
FBgn0262619	DNAlig1	none	none
FBgn0259113	DNApol	none	none
FBgn0264326	DNApol	none	none
FBgn0002905	DNApol	none	none
FBgn0263600	DNApol	none	none
FBgn0002183	dre4	none	none
FBgn0000996	dup	some	dup;Pms2
FBgn0087008	e(y)3	some	e(y)3
FBgn0087008	e(y)3	some	no Dmel match
FBgn0000615	exu	some	exu
FBgn0033354	FANCI	some	CG33680;FANCI
FBgn0005390	fs(1)M3	none	none
FBgn0004650	fs(1)N	none	none
FBgn0001085	fz	all	fz
FBgn0283682	Ge	none	none
FBgn0015391	glu	none	none
FBgn0266580	Gp210	none	none
FBgn0261278	grp	some	grp
FBgn0283499	InR	none	none
FBgn0011604	Iswi	none	none
FBgn0015396	jumu	some	jumu
FBgn0030268	Klp10A	some	Klp10A;Klp59C;Klp59D
FBgn0038476	kuk	none	none
FBgn0034657	LBR	some	LBR
FBgn0019686	lok	all	lok
FBgn0283521	lola	some	no Dmel match
FBgn0283521	lola	some	pre
FBgn0039972	Marf1	some	Marf1
FBgn0025743	mbt	some	mbt
FBgn0014861	Mcm2	some	Mcm2
FBgn0284442	Mcm3	some	Mcm3
FBgn0017577	Mcm5	none	none
FBgn0025815	Mcm6	none	none
FBgn0020633	Mcm7	none	none
FBgn0004419	me31B	all	me31B
FBgn0261786	mi	none	none
FBgn0036486	Msh6	some	Msh6
FBgn0010431	mtrm	some	no Dmel match
FBgn0002872	mu2	some	mu2
FBgn0002873	mud	none	none
FBgn0002878	mus101	none	none
FBgn0002924	ncd	none	none
FBgn0029970	Nek2	some	Nek2
FBgn0032848	nesd	all	nesd
FBgn0002962	nos	all	nos
FBgn0039559	NSD	none	none
FBgn0021761	Nup154	none	none
FBgn0033766	Nup188	some	Nup188
FBgn0031078	Nup205	none	none
FBgn0034310	Nup75	all	Nup75
FBgn0004882	orb	some	orb
FBgn0003015	osk	none	none
FBgn0003028	ovo	some	no Dmel match
FBgn0003044	Pcl	none	none
FBgn0261811	pico	some	pico
FBgn0004872	piwi	none	none
FBgn0036354	Poc1	some	Poc1
FBgn0003124	polo	some	polo
FBgn0003165	pum	some	tna
FBgn0261987	Pxt	none	none
FBgn0003187	qua	none	none

Table S6: Core ovary genes. *(continued)*

Dmel parent gene ID	Dmel parent gene symbol	transcripts in homology group	homology group Dmel sequence symbols
FBgn0003346	RanGAP	all	RanGAP
FBgn0039644	rdog	none	none
FBgn0264493	rdx	some	rdx
FBgn0040290	RecQ4	some	CG6888;Jafrac1;Jafrac2;Prx3;RecQ4
FBgn0020379	Rfx	some	Rfx
FBgn0034249	RhoGAP54D	some	RhoGAP54D
FBgn0034249	RhoGAP54D	some	dgt3
FBgn0050085	Rif1	some	Rif1
FBgn0250850	rig	none	none
FBgn0011703	RnrL	some	RnrL
FBgn0003268	rod	some	rod
FBgn0025802	Sbf	none	none
FBgn0032475	Sfmbt	none	none
FBgn0003401	shu	some	shu
FBgn0051163	SKIP	some	SKIP
FBgn0016070	smg	some	CG5280;smg
FBgn0016070	smg	some	no Dmel match
FBgn0037025	Spc105R	none	none
FBgn0027500	spd	none	none
FBgn0003483	spn	none	none
FBgn0033348	Spt	some	Spt;Sry
FBgn0262733	Src64B	none	none
FBgn0002466	sti	none	none
FBgn0052676	stx	some	stx
FBgn0003655	swa	all	swa
FBgn0031030	Tao	none	none
FBgn0003701	thr	none	none
FBgn0284220	Top2	none	none
FBgn0033636	tou	none	none
FBgn0041775	tral	some	tral
FBgn0086356	tum	some	Echs1;RacGAP84C;tum
FBgn0260780	wisp	some	wisp
FBgn0039338	XNP	some	XNP
FBgn0039338	XNP	some	no Dmel match
FBgn0004649	yl	none	none
FBgn0259789	zld	some	no Dmel match

Table S7: Core head genes.

Dmel parent gene ID	Dmel parent gene symbol	transcripts in homology group	homology group Dmel sequence symbols
FBgn0261788	Ank2	none	none
FBgn0000120	Arr1	all	Arr1;Arr2;krz
FBgn0000121	Arr2	some	Arr1;Arr2;krz
FBgn0000206	boss	all	boss
FBgn0264386	Ca	none	none
FBgn0263111	cac	none	none
FBgn0015609	CadN	none	none
FBgn0053653	Cadps	none	none
FBgn0013759	CASK	none	none
FBgn0035720	CG10077	none	none
FBgn0039927	CG11155	none	none
FBgn0033250	CG14762	some	CG14762
FBgn0052432	CG32432	none	none
FBgn0263077	CG43340	none	none
FBgn0029834	CG5937	none	none
FBgn0035253	CG7971	some	CG7971
FBgn0040502	CG8343	some	no Dmel match
FBgn0267435	chp	none	none
FBgn0000346	comt	none	none
FBgn0285925	Fas1	some	Fas1
FBgn0259108	futsch	none	none
FBgn0027575	GABA	some	GABA
FBgn0004435	Galphaq	some	CG17760;CG30054;Galphai;Galphao;Galphaq;Galphas
FBgn0004623	Gbeta76C	some	Gbeta13F;Gbeta5;Gbeta76C
FBgn0010114	hig	some	hig
FBgn0031294	IA	some	IA
FBgn0004784	inaC	none	none
FBgn0261794	kcc	some	kcc
FBgn0000464	Lar	none	none
FBgn0267429	lovit	some	lovit;Slc45
FBgn0085434	NaCP60E	none	none
FBgn0002938	ninaC	none	none
FBgn0002940	ninaE	some	ninaE;Rh2;Rh6
FBgn0262738	norpA	none	none

Table S7: Core head genes. *(continued)*

Dmel parent gene ID	Dmel parent gene symbol	transcripts in homology group	homology group Dmel sequence symbols
FBgn0032946	nrv3	some	nrv1;nrv2;nrv3
FBgn0038975	Nrx	some	Spn88Ea;Spn88Eb
FBgn0259994	OtopLa	some	OtopLa
FBgn0285944	para	none	none
FBgn0011693	Pdh	some	Pdh
FBgn0264598	PsGEF	some	no Dmel match
FBgn0263102	psq	some	psq
FBgn0003249	Rh3	some	Rh3;Rh4;Rh5
FBgn0003250	Rh4	all	Rh3;Rh4;Rh5
FBgn0004574	Rop	none	none
FBgn0003392	shi	none	none
FBgn0267001	Ten	none	none
FBgn0030412	Tomosyn	some	CSN1a;CSN1b
FBgn0003861	trp	none	none
FBgn0025726	unc	none	none
FBgn0267002	unc	none	none
FBgn0038693	unc79	none	none
FBgn0039536	unc80	none	none

References

1. Leader, D. P., Krause, S. A., Pandit, A., Davies, S. A. & Dow, J. A. T. FlyAtlas 2: A new version of the *Drosophila melanogaster* expression atlas with RNA-seq, miRNA-seq and sex-specific data. *Nucleic Acids Research* **46**, D809–D815 (2018).

2. Larkin, A. *et al.* FlyBase: Updates to the *Drosophila* melanogaster knowledge base. *Nucleic Acids Research* **49**, D899–D907 (2021).